Strike-slip tectonics and Quaternary basin formation along the Vienna Basin fault system inferred from Bouguer gravity derivatives

B. C. Salcher, B. Meurers, J. Smit, K. Decker, M. Hölzel, M. Wagreich

Strike-slip tectonics and Quaternary basin formation along the Vienna Basin fault system inferred from Bouguer gravity derivatives

B. C. Salcher,[1] B. Meurers,[2] J. Smit,[3] K. Decker,[4] M. Hölzel,[5] and M. Wagreich[4]

Received 30 June 2011; revised 21 March 2012; accepted 27 March 2012; published 8 May 2012.

[1] The Vienna Basin at the transition between the Alpine and Carpathian belt hosts a number of large Pleistocene sub-basins forming along an active continental scale strike-slip fault (Vienna Basin strike-slip fault). We utilize first-order derivatives from industrial Bouguer gravity data to unravel the impacts of Pleistocene kinematics on the Vienna Basin and to compensate for the lack of near-surface fault data. Anomalies have been evaluated by independent geophysical and geological data and were integrated to build up a tectonic model. Factors influencing the wavelength and the amplitude of anomalies were additionally investigated by 2-D models to better interpret field data. Subsidence and related accumulation of Quaternary sediments in the Vienna Basin produce significant gravity signals related to the activity of the strike-slip fault. The constrained fault patterns and structures highlight tight and elongated transtensional pull-apart basins with typically associated features like separated depocenters and Riedel fractured sidewalls in an en-echelon alignment. Further Pleistocene basins are highlighted as tectonic grabens developing along branches of the master fault. The Vienna Basin is additionally affected by minor deformation represented by both subsidence along major Miocene sidewalls and NW-SE faulting resulting in distinct topographic features, which manifests kinematics on a regional scale. The clear density contrasts between Miocene marine and Quaternary terrestrial sediments, as well as the exceptional database, provide a unique framework to demonstrate advantages of incorporating gravity derivatives for near-surface fault analysis.

Citation: Salcher, B. C., B. Meurers, J. Smit, K. Decker, M. Hölzel, and M. Wagreich (2012), Strike-slip tectonics and Quaternary basin formation along the Vienna Basin fault system inferred from Bouguer gravity derivatives, *Tectonics*, *31*, TC3004, doi:10.1029/2011TC002979.

1. Introduction

[2] The Vienna Basin (Figure 1) is one of the world's most studied pull-apart basins [e.g., *Royden*, 1985; *Wessely*, 1988; *Fodor*, 1995; *Decker et al.*, 2005; *Wu et al.*, 2009]. It formed as a thin-skinned pull-apart basin along a stepover of a major sinistral fault system at the transition between the Eastern Alps and the Western Carpathians. Formation of the Vienna Basin is the consequence of eastward lateral extrusion of a major Alpine-Carpathian block in the Middle and Late Miocene [*Ratschbacher et al.*, 1991a, 1991b; *Decker and Peresson*, 1996; *Linzer et al.*, 2002]. Recent activity is associated with moderate seismicity along the Vienna Basin strike-slip fault (VBSSF) [e.g., *Gutdeutsch and Aric*, 1988; *Schenková et al.*, 1998] (Figure 1) expanding from the Mur-Mürz fault in the Eastern Alps, throughout the Vienna Basin into the westernmost Carpathians (Malé Karpaty). Strike-slip kinematics of this fault is related to subsidence along a chain of releasing bends within the Vienna Basin active since c. 300 ka [*Salcher*, 2008]. These form narrow transtensional pull-apart basins and grabens along associated splay faults [*Decker et al.*, 2005; *Salcher and Wagreich*, 2010]. Knowledge of Quaternary faulting is sparse, typically limited to local geophysical surveys, even though the Vienna Basin is home of an exceptional database including log, seismic and gravity data as it hosts giant hydrocarbon fields [*Fuchs and Hamilton*, 2006]. Coverage of industrial data is, with the exception of Bouguer gravity, typically clustered in regions of economic interest and limited in the top hundreds of meters [*Brix and Schulz*, 1993]. Bouguer gravity surveys are typically carried out on a basin scale [e.g., *Granser*, 1987; *Rousset et al.*, 1993; *Lefort and Agarwal*, 1996; *Lopes Cardozo et al.*, 2005; *Rotstein et al.*, 2006; *Szafián and Horváth*, 2006] and can be utilized to enhance features related to shallow structures [e.g., *Blakely*,

[1]Department of Earth Sciences, ETH-Zurich, Zurich, Switzerland.
[2]Department of Meteorology and Geophysics, University of Vienna, Vienna, Austria.
[3]ISTeP, Université Pierre et Marie Curie, Paris, France.
[4]Department of Geodynamics and Sedimentology, University of Vienna, Vienna, Austria.
[5]Rohoelaufsuchungs AG, Vienna, Austria.

Corresponding author: B. C. Salcher, Department of Earth Sciences, ETH-Zurich, NO E 45, Sonneggstr. 5, CH-8092 Zürich, Switzerland. (bernhard.salcher@erdw.ethz.ch)

0278-7407/12/2011TC002979

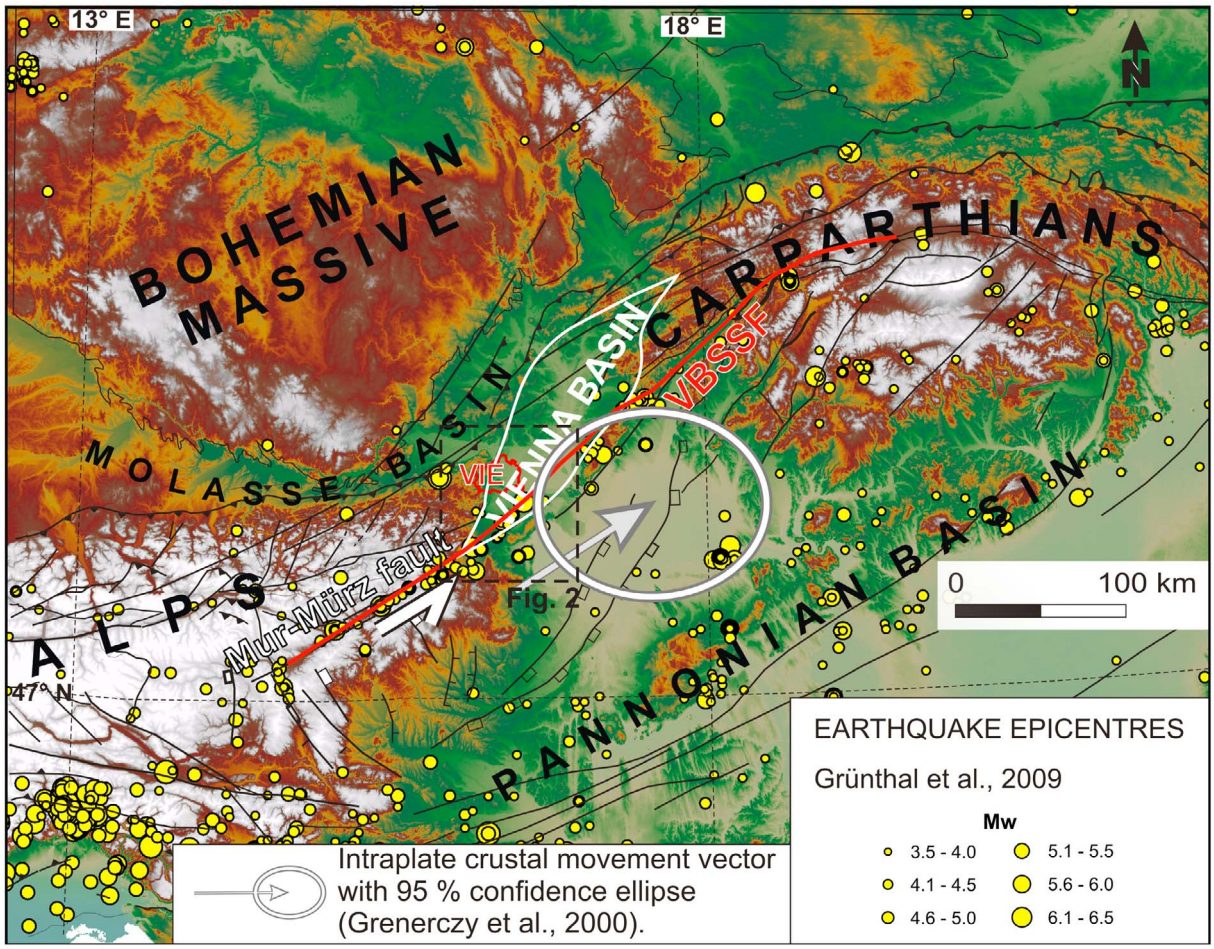

Figure 1. Tectonic and topographic overview of the Vienna Basin and its vicinity. Seismic activity in the Alpine Carpathian transition is focused along the Vienna Basin strike-slip fault (VBSSF) extending from the Mur-Mürz valley to the eastern part of the Vienna Basin and the Western Carpathians. Intraplate crustal movement vector from *Grenerczy et al.* [2000] (c. 1.5 mm/a).

1995]. By calculating first-order derivatives in the horizontal (HG) or vertical direction (VG) of the gravity field, near-surface changes are highlighted constraining i.e., fault-separated lithologies with different density [e.g., *Zeng*, 1989; *Ten Brink et al.*, 1993; *Ben-Avraham et al.*, 1996; *Achmon and Ben-Avraham*, 1997; *Sedlák et al.*, 2001; *Lopes Cardozo et al.*, 2005; *Büyüksaraç et al.*, 2005; *Rotstein et al.*, 2006; *Reynisson et al.*, 2007; *Rajchl et al.*, 2009]. The lack of fault trace information is a common problem in sedimentary basins where only point (drilling) or cross-sectional data (2-D seismic) is available. The application of gravity derivatives may compensate for this deficit. Even though first-order derivatives are especially utilized to highlight faults in sedimentary basins, factors influencing the wavelength and the amplitude of derivatives remain often poorly investigated due to sparse geophysical data. High density contrasts between Vienna Basin's Miocene and Pleistocene basin fill as well as comprehensive data provide a unique framework to test the characteristics of Bouguer gravity's derivatives and its relation to near-surface structures. In this study, we (i) investigate the significance of Bouguer gravity's derivatives to detect shallow structures in basins, both theoretically and by independent geological and geophysical data, and (ii) utilize gravity data to build up a tectonic model of the Quaternary Vienna Basin. It is not our intention to perform gravity density modeling but rather to apply gravity derivatives as a simple tool to enhance near-surface information in sedimentary basins.

[3] We provide new and detailed insights in the tectonics and recent basin forming processes of the Vienna Basin. The study focuses on the Austrian part of the Vienna Basin where highest Quaternary activity is evident and comprehensive data sets are accessible.

2. The Evolution of the Vienna Basin Since the Middle Miocene

2.1. The Miocene Vienna Basin

[4] The Vienna basin is a thin-skinned pull-apart basin on top of the Alpine-Carpathian fold-thrust belt [*Royden*, 1985; *Wessely*, 1988; *Decker*, 1996; *Decker and Peresson*, 1996]. Extension and basin subsidence initiated in the Middle Miocene (c. 16 Ma) after the termination of fold-thrusting [*Hölzel et al.*, 2010] and at the onset of lateral extrusion along the VBSSF. The pull-apart evolved in approximate temporal coincidence with extension and transform faulting in the

Intra-Carpathian/Pannonian Basin System [*Royden et al.*, 1982; *Csontos et al.*, 1992; *Tari et al.*, 1992; *Horváth*, 1993].

[5] Sinistral strike-slip movement along a left-step of the Mur-Mürz (Figure 1) and Vienna Basin Fault System formed an about 150 km long pull-apart with a maximum width of c. 40 km [*Wessely*, 1988]. Subsidence led to the deposition of up to 4.3 km of mainly marine and brackish sediments [e.g., *Wessely*, 1988; *Hölzel et al.*, 2008]. The major normal faults formed at the basin's western boundary with peak activity during the Middle Miocene. The Late Miocene kinematics differs significantly from those during earlier stages of basin formation. In that time strike-slip activity, which was associated with the formation of extensional sinistral strike–slip duplexes and negative flower structures shifted to the eastern side of the basin [*Beidinger and Decker*, 2011]. Surface uplift caused the regression of the Paratethys sea toward SE [*Jiřiček and Seifert*, 1990] leading to terrestrial conditions around the latest stages of the Miocene [*Harzhauser et al.*, 2004; *Harzhauser and Tempfer*, 2004]. The almost complete absence of uppermost Pannonian and Pliocene sediments and kinematic data indicates a cessation of tectonic subsidence around that time [*Peresson and Decker*, 1997]. Sinistral strike-slip faulting at the Vienna Basin Transfer Fault System recurred during the Pleistocene as shown by the formation of two major Pleistocene sedimentary basins along the strike-slip fault system (Mitterndorf and Lassee Basin) [*Decker et al.*, 2005]. The reason for the tectonic quiescence during the Pliocene and the subsequent recurrence during the Middle Pleistocene is unknown. In the current tectonic regime the fault accommodates the NW-directed lateral escape of a crustal block (Styria-West Carpathian Wedge) out of the Alpine convergence zone [*Gutdeutsch and Aric*, 1988]. Recent studies on the crustal and lithospheric structure at the Alpine-Carpathian-Pannonian junction confirm these previous interpretations and highlight the Vienna Basin Fault System as one of the major faults compensating active lateral escape [*Brückl et al.*, 2010]. Active sinistral fault slip is proved by moderate seismicity, focal plane solutions and GPS data [e.g., *Reinecker and Lenhardt*, 1999; *Grenerczy et al.*, 2000; *Decker et al.*, 2005]. Incision into Miocene basin fill and the formation of Quaternary staircase terraces at the Danube River and its tributaries [*Fink and Majdan*, 1954] suggests that Pleistocene and active strike-slip faulting is occurring together with continuously low regional uplift.

2.2. The Quaternary Sub-Basins of the Vienna Basin

[6] Around c. 300 ka, activity in the Vienna Basin resumed along the Vienna Basin strike-slip fault (VBSSF) (Figure 1) [*Salcher*, 2008], which extends from the Alpine Mur-Mürz Valley to the Vienna Basin and the Vah valley in the Western Carpathians. Sinistral movement along the VBSSF is evident from seismic activity [*Reinecker and Lenhardt*, 1999; *Grünthal et al.*, 2009] and geodetic data [*Höggerl*, 1980; *Grenerczy et al.*, 2000, 2006]. Subsidence in the Vienna Basin is related to the formation of pull-apart basins (Mitterndorf, Lassee, Zohor, Pernek and Sološnica basin) and two smaller grabens in the central part (Obersiebenbrunn and Aderklaa Basin) (Figure 2). The half-grabens are argued to be kinematically linked to the VBSSF via fault splays [*Decker et al.*, 2005].

[7] The pull-aparts develop between offset segments (principal displacement zones; PDZs) of the VBSSF. The largest and deepest of these basins is the Mitterndorf Basin, located south of the Danube River. It covers 270 km^2 and is filled with up to 175 m of Quaternary sediments acting as one of Europe's largest groundwater reservoirs. The Quaternary basin fill reflects a distinct cyclicity with thick sequences of coarse sediments deposited during cold periods and thin sequences of channel and flood sediments deposited during warm periods [*Salcher et al.*, 2010]. Sediments derive generally from local Alpine catchments. In contrast, basins north of the Danube (Aderklaa, Obersiebenbrunn and Lassee) are filled with coarse gravels and occasionally overbank fines of the Danube, unconformable overlying Neogene sediments which are mostly marine. The maximum thickness of the Pleistocene fill is c. 25, 50 and 120 m, for the Aderklaa, Obersiebenbrunn and Lassee Basin, respectively [*Gangl*, 1993; *Darsow et al.*, 2009].

[8] The Mitterndorf and Lassee pull-aparts overly the negative flower structures of the Late Miocene rooting in PDZs of 3 – 5 km depth; the upward branching fault splays were at least partly reactivated during the Quaternary [*Hinsch et al.*, 2005; *Beidinger and Decker*, 2011].

3. Input Data and Methods

[9] As our primary target in this paper is to show how Bouguer gravity derivatives can be utilized to reliably constrain near-surface structures in the Quaternary Vienna Basin we first analyzed derivatives by (i) testing its theoretical behavior on various normal fault settings and by (ii) assessing anomalies with independent geological and geophysical field data.

3.1. Bouguer Gravity Data

[10] The gravity measurements of the Vienna Basin were distributed regularly with a station interval of c. 450 m [*Zych et al.*, 1993]. The interpolation between stations was performed by applying a common kriging procedure with 300 m grid spacing. We use the potential field derivatives (first-order derivatives; VG and HG) to enhance the high-frequency parts of Bouguer gravity signals and to depict near-surface sources [e.g., *Blakely*, 1995]. Point related information from derivatives have been interpolated (kriged) to trace the maxima of the first-order derivatives.

3.2. Density Contrasts in the Field and in the VG, HG Models

[11] We first tested the response to various normal fault scenarios by numerical 2-D models to better understand factors controlling VG and HG maxima in the field (Figure 4). Normal fault geometries have a constant density contrast between the hanging wall and footwall of 400 kg/m^3; 400 kg/m^3 is a rough estimate derived from the mean density contrast between Neogene and Pleistocene sediments in the field. Such a difference is sufficient enough to produce clear amplitudes.

[12] The mean density values are obtained from numerous core samples (courtesy of OMV Corporation). The sediment density obtained from the Vienna Basin's Neogene basin ranges between c. 2600 kg/m^3 for marine sands and 2800 kg/m^3 for cemented conglomerates close to the basement in a depth of

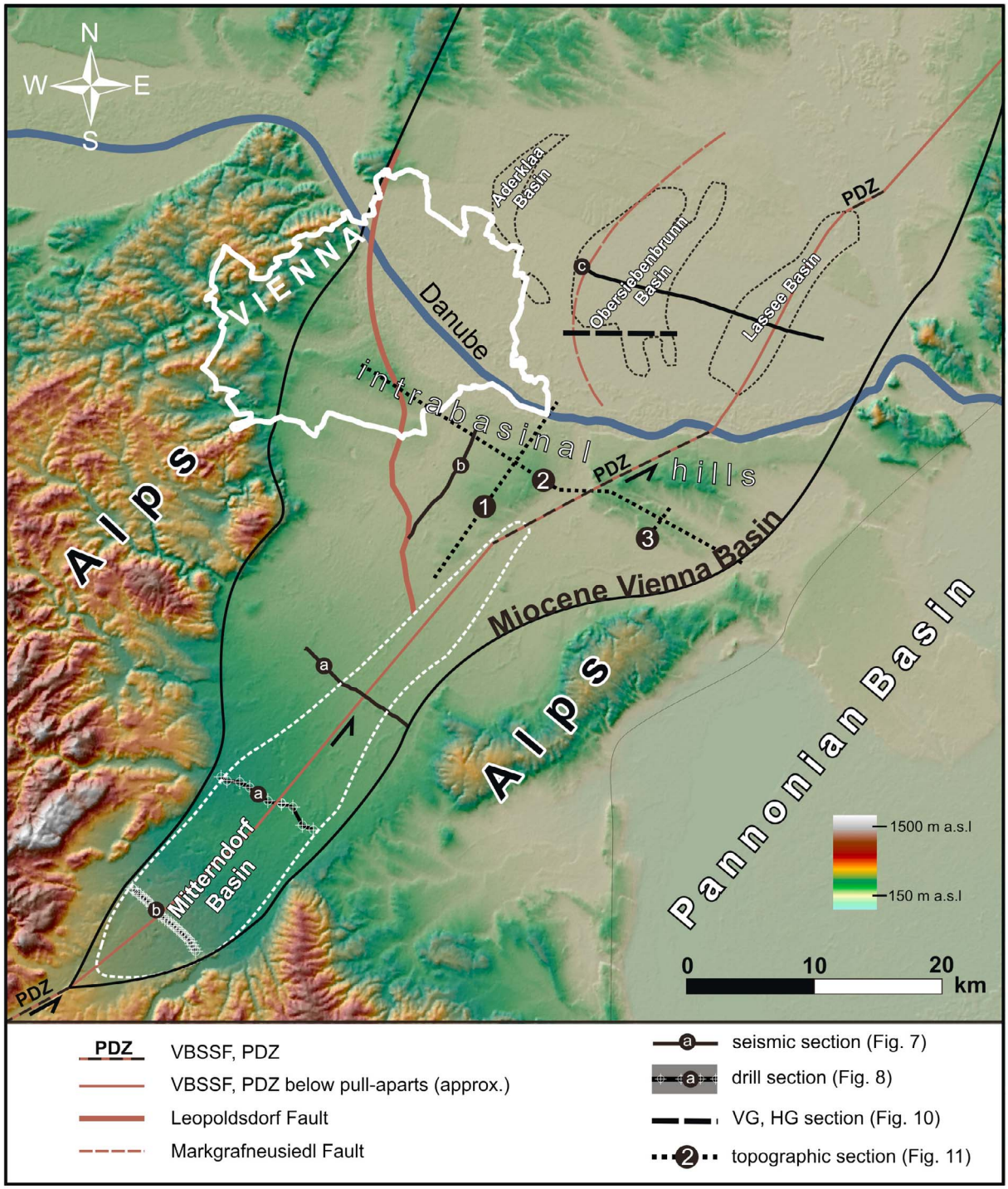

Figure 2. The Miocene Vienna Basin, the locations of its Pleistocene sub-basins and major faults. Pull-aparts (Mitterndorf and Lassee Basin) develop between offset principal displacement zones (PDZs). The approximate outlines of Pleistocene Basins are drawn after *Gangl* [1993] and *Salcher and Wagreich* [2010]. Positions of seismic (Figure 7), drilling (Figure 8), VG/HG (Figure 10) and topographic (Figure 11) sections are indicated.

several 1000 m. Data for near-surface, Late Miocene fluvial and deltaic deposits of the Paleo-Danube (with thicknesses of up to several tens of meters) do not exist but must be clearly lower as consolidation degree is similar to Pleistocene sediments (Figure 3). The maximum measured density of Pleistocene sediment is c. 2300 kg/m^3 (Middle Pleistocene massive gravels in the Mitterndorf Basin at a depth of 40 m). Even though a database with precise densities of Pleistocene basin sediments is lacking, no significant density variations within Quaternary sediments are expected considering the

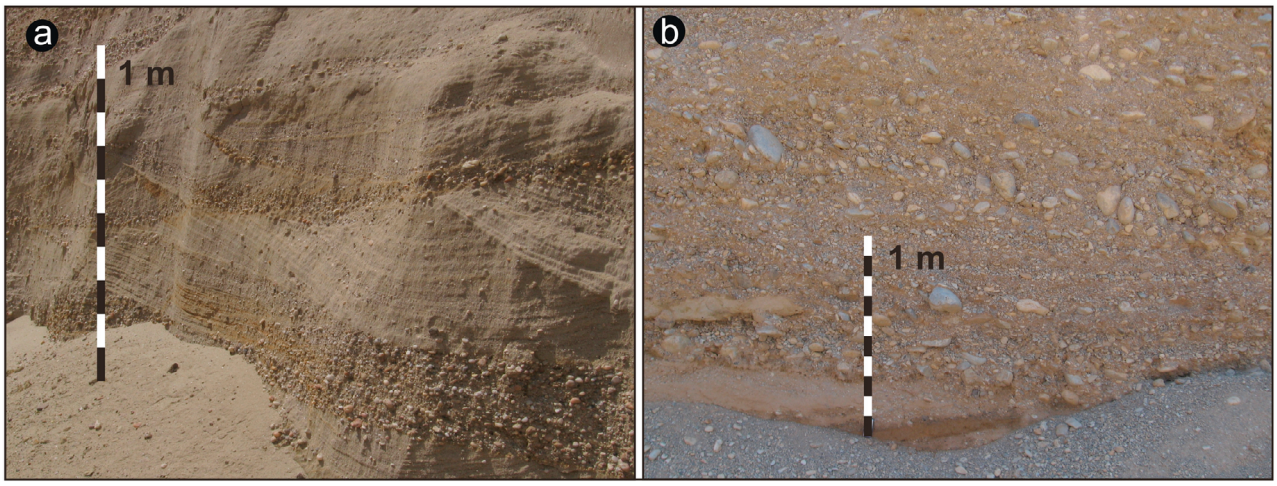

Figure 3. (a) Late Miocene deltaic deposits of the Danube (intrabasinal hills) and (b) massive, Late Pleistocene gravels deposited by a Danube tributary (Mitterndorf Basin). Consolidation degree (and density) of both facies is low. Sediments overly consolidated, clayey to fine sandy marine sediments of the Paratethys.

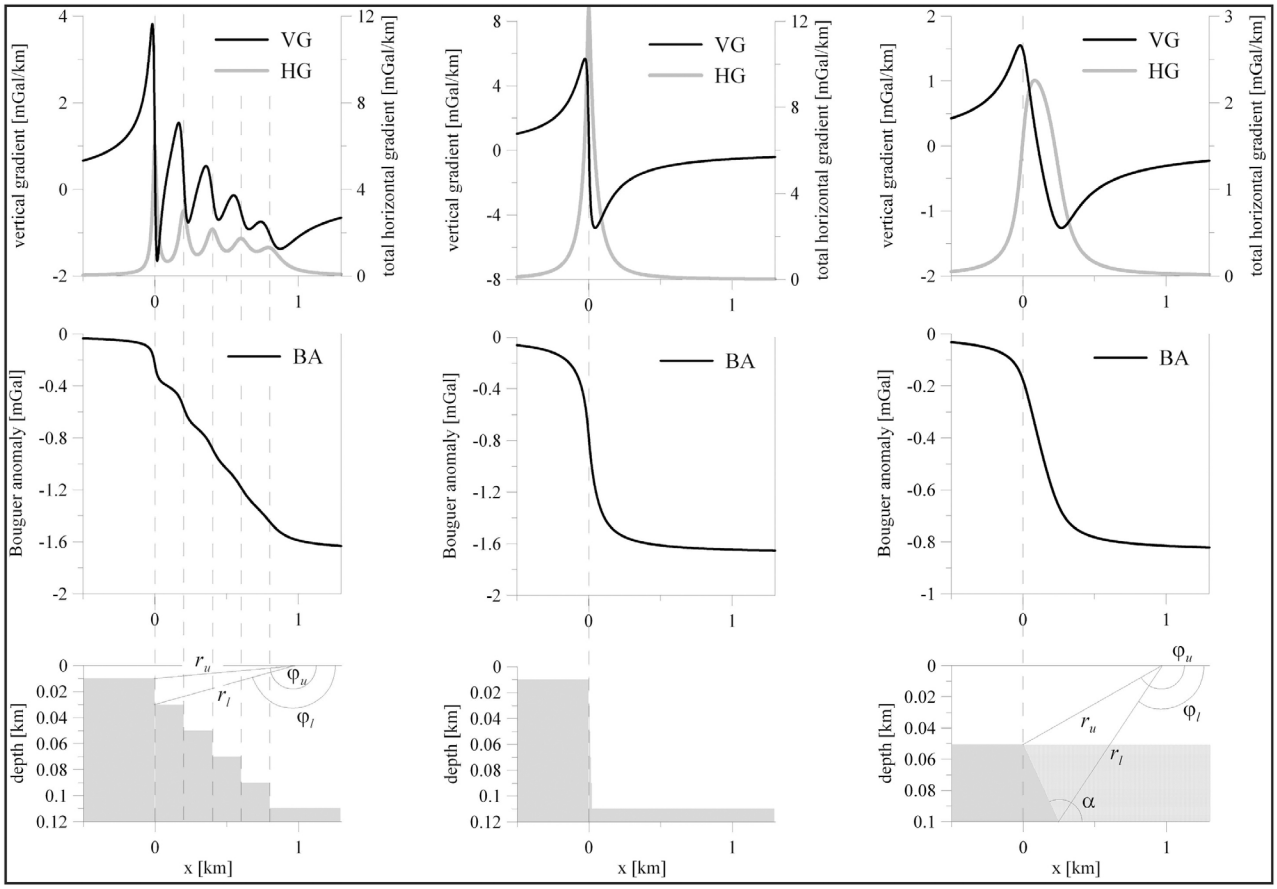

Figure 4. Models showing the behavior of VG and HG at different vertical displacement scenarios using a constant density difference between the hanging and footwall of 400 kg/m^3. (left) Near-surface faults with low vertical displacements in an en-echelon pattern. VG and HG maxima are distinctly decreasing; displacements of both signals become larger with depth of individual faults. (middle) A sub-vertical, single fault in which the VG and HG have highest maxima due to a high vertical displacement. (right) Representation of a deeper structure with a larger dip. VG and HG maxima are the lowest and wavelength is longest due to the depth and the dip of the fault. See text for details.

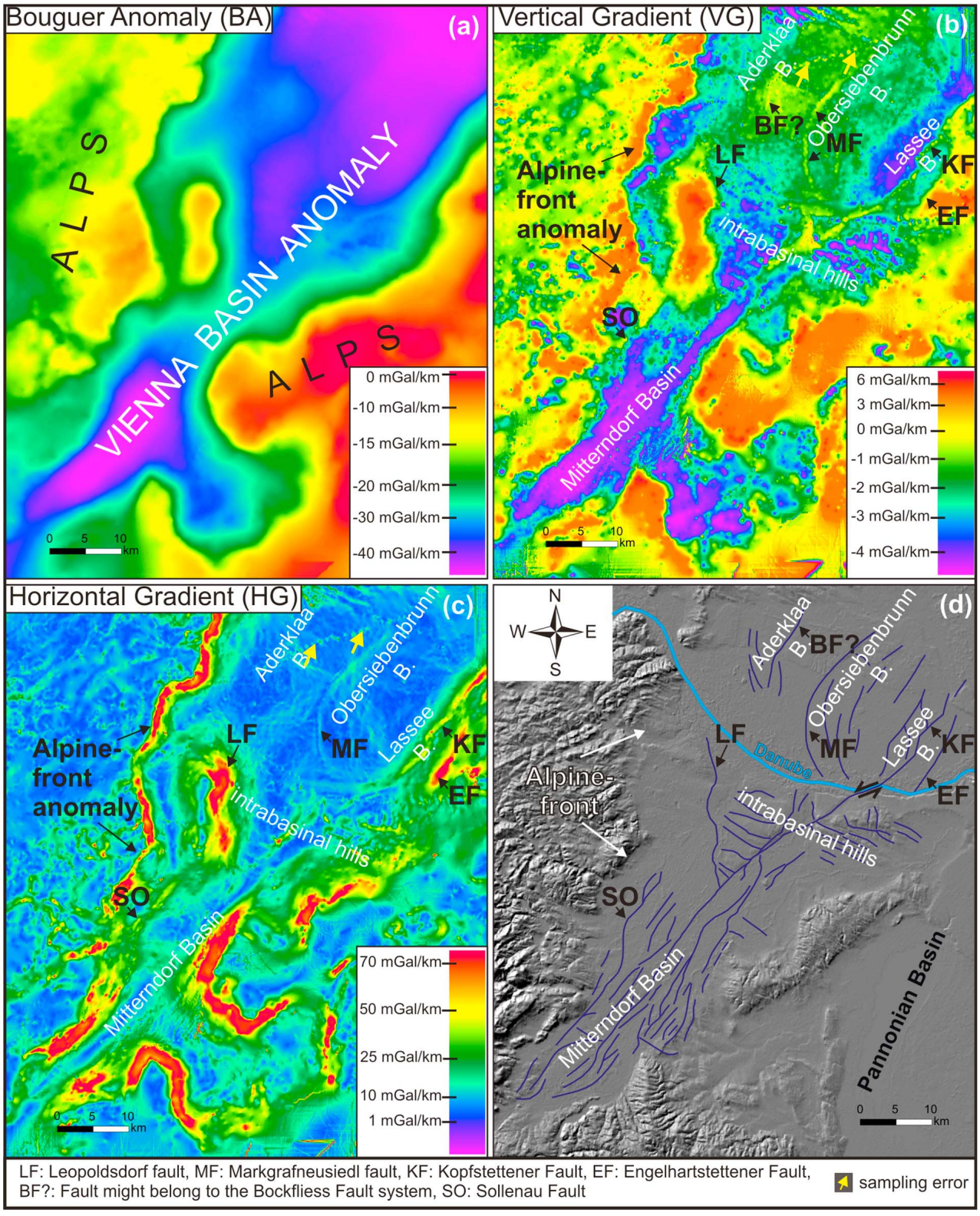

Figure 5. (a) Complete Bouguer Anomaly, (b) VG, (c) HG and normal faults represented by (d) VG maxima superimposed on a hill-shaded DEM of the southern and central Vienna Basin (Austrian part of the Vienna Basin). The location of active Pleistocene basins is shown. See text and Figures 7 and 8 for details. Middle Miocene Faults which are relevant since the early phase of the Vienna Basin are indicated.

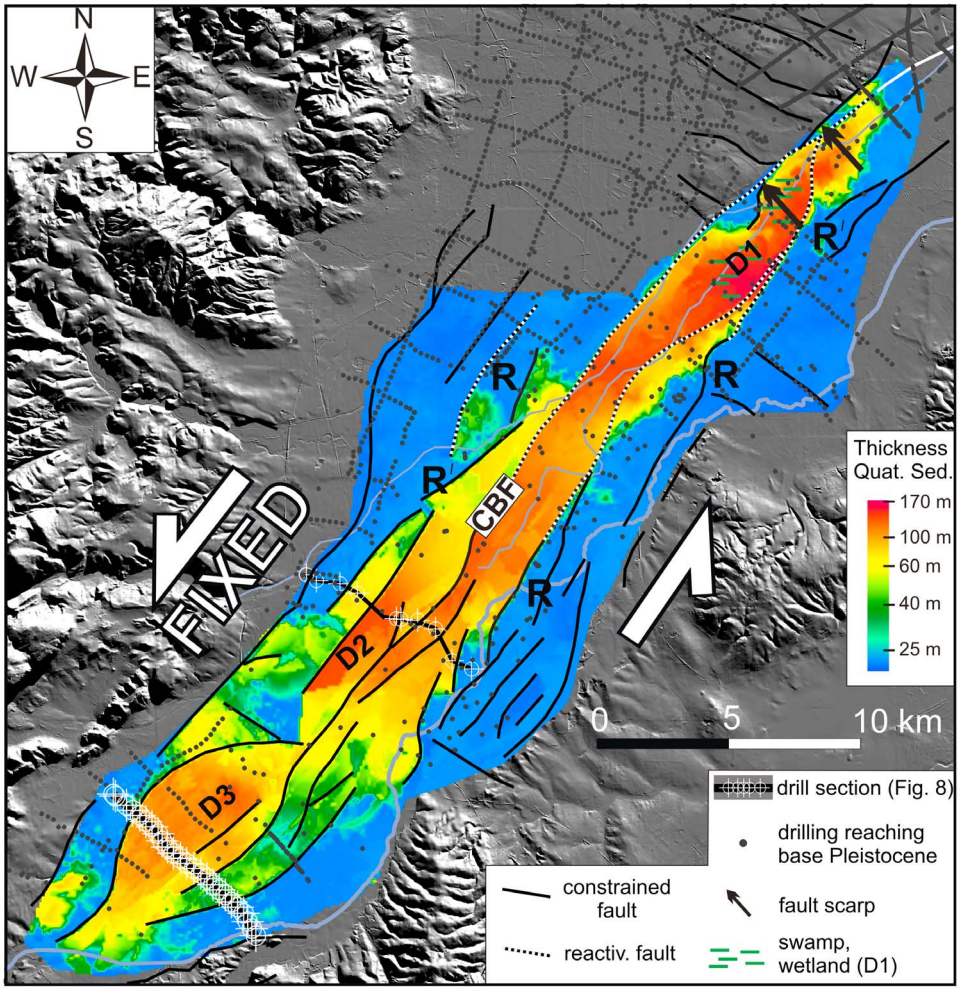

Figure 6. Faults and thickness of Quaternary sediments in the Mitterndorf Basin calculated by applying an inverse distance algorithm [*Shepard*, 1968] using ~800 drillings. Mapped maxima of the VG constrained as faults act as break lines for the interpolation routine. Active Quaternary faults are associated with growth of sediments. Anomalies not associated with sediment growth depict inactive Miocene faults at near-surface positions. The three depocenters are marked as D1, D2 and D3 developing along a cross-basin fault zone (CBF). Movement along the VBSSF is related to the block east of the cross-basin fault zone only. Faults marked "R" have the orientation of Riedel (R) and anti-Riedel fractures (R′) in a sinistral fault zone. Dashed black and white lines mark Miocene faults, which are reactivated during the Quaternary indicated from 2-D (Figure 6a) and 3-D seismic (along D1) [*Hinsch et al.*, 2005]. Note that these lines are only drawn in areas covered by high resolution reflection seismic. There is no seismic coverage SW of these lines. Occurrences of wetland and peat deposits in the north mark the position of a sag pond, which is bounded by a fault scarp in the west (black arrows). Map is not smoothed: where drilling density is low, interpolation shadows (clear change in color) and strong local changes of thickness do occur.

lateral and vertical homogeneity of massive deposits [*Salcher and Wagreich*, 2010].

3.3. Fault Constraint: VG, HG Mapping Procedure, Thresholds and Assessment Data

[13] The fault pattern presented in this paper is based on the VG maximum which most closely captures the fault's cut off line (Figure 4). The assessment of geological and geophysical data indicate that changes in the gravity field can be reliable attributed to normal faults if (i) the VG maximum is larger than c. 0.5 mgal/km and (ii) the trace of the anomaly is in the order of several kilometers (Figures 7–10). Hence, a minimum value of 0.5 mgal/km has been taken for mapping of normal faults in the Pleistocene basins. The traceable VG maximum (the fault trace) was not mapped below c. 2 km. Somewhat lower VG values (between 0.25 and 0.5 mgal/km) have been assessed in the south (Figure 6). Such low values, however, were only incorporated if, and only if, independent data confirmed the specific anomaly indicating a normal fault.

[14] Assessment data south of the Danube included log data, industrial 2-D and 3-D reflection seismic as well as geoelectric measurements (Table 1). Assessment data north of the Danube included structural maps of the Top Neogene,

Table 1. Coverage of Geophysical, Geological, and Topographic Data[a]

Data	Coverage	Origin
DEM 10 m	complete	Fed. Office Metrology and Surveying
Bouguer gravity	complete	OMV, Fed. Office Metrology and Surveying
Drill logs (c. 2000)	SD	OMV, Geol. Survey
2-D seismic (8 sections)	MB, middle – northern part (6), IH (2)	OMV
3-D seismic (1 cube)	MB, northern part	OMV; *Hinsch et al.* [2005]
Geoelectrics (c. 20 sections)	MB	*Berger* [1989]; *Prohaska* [1983]
Top Neogene	ND	OMV; *Gangl* [1993]
Top Middle Miocene	ND, IH	OMV; *Unterwelz* [1993]
Top Alpine (pre-Neogene) Basement	complete	OMV; *Kröll and Wessely* [1993]

[a]MB: Mitterndorf Basin, IH: Intrabasinal hills, SD: area south of the Danube (IH included), ND: area north of the Danube. Data courtesy OMV cooperation, Federal Office of Metrology and Surveying, Geological Survey of Austria.

Top Middle Miocene and Top pre-Neogene (Alpine) Basement. Here, 2-D seismic data was available from the study of *Beidinger and Decker* [2011] (e.g., Figure 7c). Three-dimensional seismic data was not accessible. Digital topographic (10 m ground resolution) and Bouguer gravity data was available for the entire study area. The clear lithologic contrast between Miocene marine and the Quaternary fluvial sediments is an important factor to constrain the location of normal faults.

3.4. Well Data

[15] Log data provide valuable information on possible locations of Pleistocene faults and their accordance with the mapped anomaly maxima. The unconformity of the Pleistocene - Neogene boundary is commonly well detectable due to the clear differences in litho facies (fluvial versus marine). Out of c. 2000 available drill logs from the area south of the Danube, c. 1200 come from the Mitterndorf Basin, including numerous deep groundwater drillings (>50 m) with precise log information. North of the Danube, accurate log data from deeper Pleistocene units are limited and were not accessible. Available Pleistocene basement maps, however, are so far based solely on drillings [*Gangl*, 1993] and limited structural input data [*Darsow et al.*, 2009].

4. Results

4.1. Modeling of VG and HG Across Normal Faults

[16] To test the behavior of vertical and horizontal gradients on different tectonic subsidence settings we applied a series of 2-D models (Figure 4). The gravity derivative calculation of *VG* and *HG* from Bouguer anomaly data can be done efficiently by potential field transformation in the frequency domain by applying fast Fourier transformation (FFT). The transformed field quantity h results from evaluating the inverse Fourier integral, where in the integral kernel appears the Fourier transform Σ of the Bouguer gravity g_3 multiplied by the filter operator Φ:

$$h(x_1,x_2)=\frac{1}{4\pi^2}\int_{-\infty}^{\infty}\int_{-\infty}^{\infty}\mathcal{F}(k_1,k_2)\mathcal{S}(k_1,k_2)\,e^{i(k_1x_1+k_2x_2)}dk_1dk_2 \quad (1)$$

where $k_{1,2}$ denote the components of the wave number vector. The following filter operators have to be used for calculating the first spatial derivatives of the Bouguer gravity:

$$\begin{aligned}&\frac{\partial g_3}{\partial x_1}:\mathcal{F}(k_1,k_2)=ik_1\\&\frac{\partial g_3}{\partial x_2}:\mathcal{F}(k_1,k_2)=ik_2\\&\frac{\partial g_3}{\partial x_3}:\mathcal{F}(k_1,k_2)=-\sqrt{k_1^2+k_2^2}\qquad\text{vertical gradient }(VG).\end{aligned} \quad (2)$$

[17] The total horizontal gradient (*HG*) of the Bouguer anomaly is then calculated by equation (3):

$$HG=\sqrt{\left(\frac{\partial g_3}{\partial x_1}\right)^2+\left(\frac{\partial g_3}{\partial x_2}\right)^2}\ \text{total horizontal gradient }(HG). \quad (3)$$

[18] First-order derivatives are especially suitable to enhance anomaly features of near-surface density contrasts, like in the setting of the Quaternary Vienna Basin with considerable density differences between hanging and footwall. Derivatives were calculated in a coordinate system with the vertical axis pointing downward by applying closed formulas for 2-D fault structures [e.g., *Militzer and Weber*, 1984; *Jung*, 1961]:

$$\begin{aligned}HG(x)&=\left|-2G\Delta\rho\ln\left(\frac{r_u}{r_l}\right)\right|\\VG(x)&=2G\Delta\rho(\varphi_l-\varphi_u)\end{aligned} \quad (4)$$

where G denotes the gravitational constant, $\Delta\rho$ is the density contrast. r_u and r_l represent the distances between gravity station and the cut off points of the hanging wall and footwall, respectively. φ_u and φ_l are the angles between the positive x-axis and the corresponding cut off points.

[19] For non-vertical faults, gradients are calculated by equation (5) [e.g., *Militzer and Weber*, 1984; *Jung*, 1961]:

$$\begin{aligned}HG(x)&=\left|2G\Delta\rho\left\{\sin\alpha\cos\alpha(\varphi_l-\varphi_u)-\sin^2\alpha\ln\left(\frac{r_u}{r_l}\right)\right\}\right|\\VG(x)&=-G\Delta\rho\left\{2\sin^2\alpha(\varphi_l-\varphi_u)+\sin\alpha\cos\alpha\ln\left(\frac{r_u}{r_l}\right)\right\}\end{aligned} \quad (5)$$

where α denotes the inclination angle of the fault (see also Figure 4).

[20] Figure 4 shows different scenarios of vertical tectonic displacement with various spacing, dip and displacement

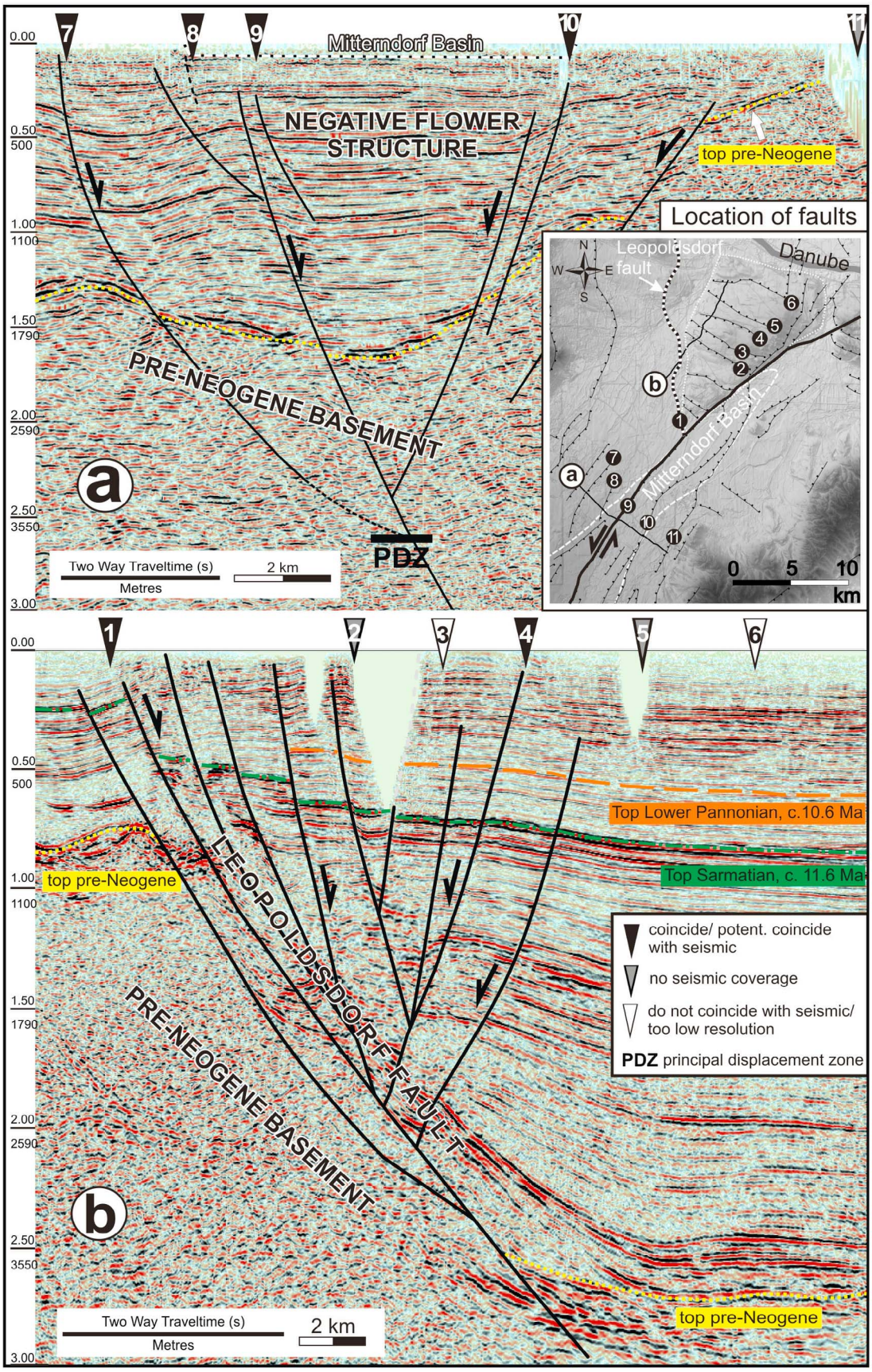
Mitterndorf Basin
NEGATIVE FLOWER STRUCTURE
top pre-Neogene
Location of faults
Leopoldsdorf fault
Danube
Mitterndorf Basin
PRE-NEOGENE BASEMENT
PDZ
Two Way Traveltime (s)
Metres
2 km
0 5 10
km
Top Lower Pannonian, c.10.6 Ma
Top Sarmatian, c. 11.6 Ma
LEOPOLDSDORF FAULT
coincide/ potent. coincide with seismic
no seismic coverage
do not coincide with seismic/ too low resolution
PDZ principal displacement zone

Figure 7

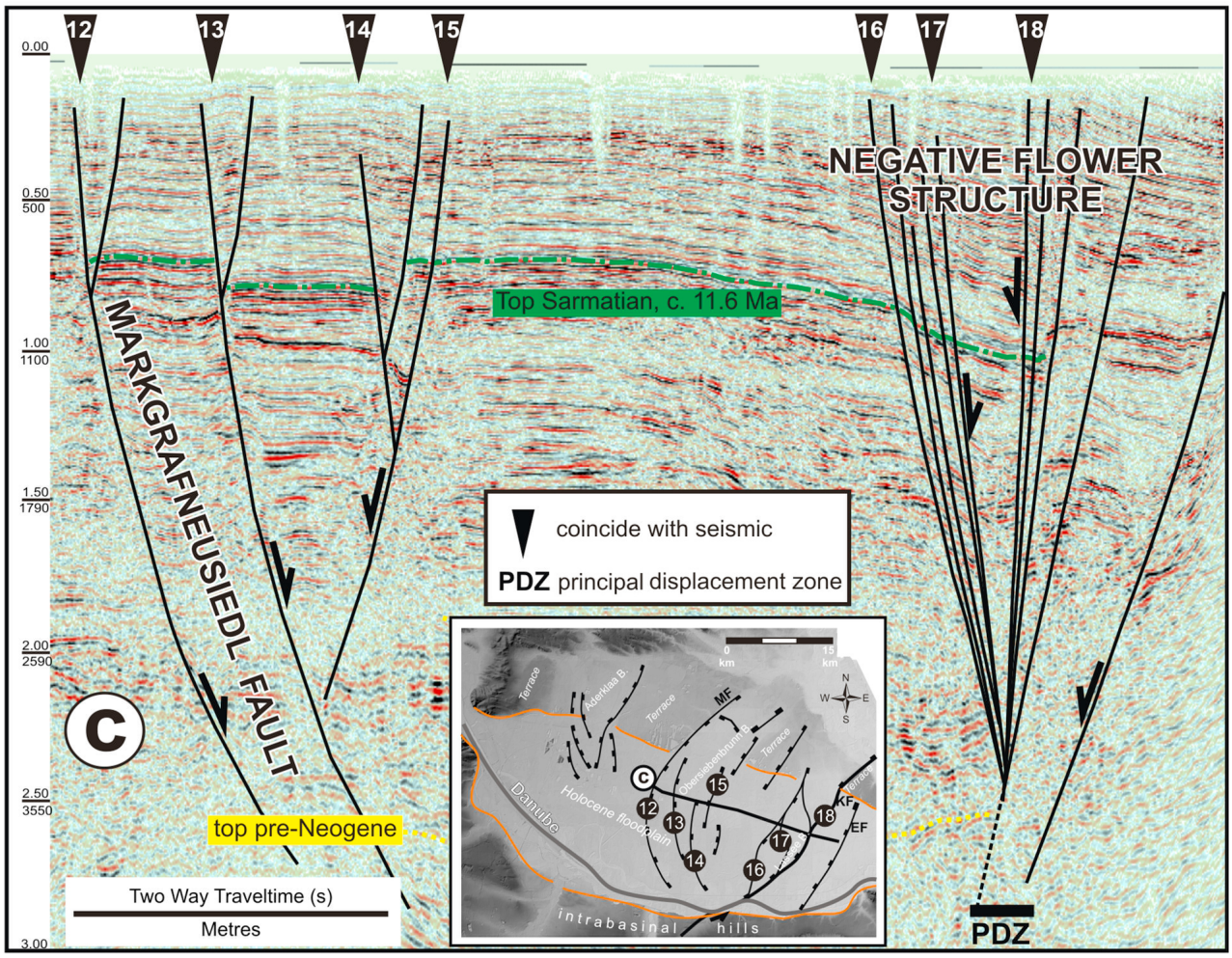

Figure 7. (continued)

distance and the response of VG and HG. Models have a constant density contrast of −400 kg/m^3 between the hanging wall and the footwall. Any change in the difference would only be manifested in the magnitude of the amplitude. The numerical models show that normal faults displacing material with constant density contrast between the footwall and hanging wall block produce a VG maximum at, or close to the footwall cutoff and a minimum at or close to the hanging wall cutoff. Both depend on the fault angle, the vertical displacement and the depth of the structure. The maximum of the HG is located at the fault heave, between the maximum and minimum of the vertical gradient. The dip direction of a fault may be assessed from the relation between the position of the VG maximum with respect to the HG maximum [*Bott*, 1962]. For near-vertical faults both maxima almost coincide, whereas both maxima are markedly offset for shallow-dipping faults. Theoretically, HG and VG show a perfect symmetrical resp. antisymmetrical signal if a fault is vertical, and their extremes would coincide if a vertical fault extends to the surface.

[21] Vertical normal faults in en-echelon pattern (Figure 4, left) produce well separated VG maxima each associated with a fault cut off. The HG maxima show a slight displacement to the VG increasing with depth. Generally, the

Figure 7. Coincidence of anomalies derived from the maxima of the VG (black triangles) with faults imaged in the industrial seismics. Seismic data does typically not fully resolve the uppermost c. 300 m. (a) Synthetic and antithetic faults of the negative flower structure below the Mitterndorf Basin. Note the inserted limits of the Mitterndorf Basin at the very top illustrating the dimension to the flower structure. Splay faults converge to depth into the principal displacement zone (PDZ) of the VBSSF. (b) NE striking synthetic and antithetic faults between the Leopoldsdorf fault and the Vienna Basin strike-slip fault (VBSSF). The profile cuts Leopoldsdorf with an oblique angle. (c) Synthetic and antithetic faults of the Obersiebenbrunn Basin (graben structure) and of the negative flower structure below the Lassee Basin (modified from *Beidinger and Decker* [2011]). Splay faults of the Lassee Basin converge to depth into the principal displacement zone (PDZ) of the VBSSF. Note that the VG maxima associated with the flower structure (16–18 and Figure 9c) represent a tight fault zone with multiple, very steep faults in an en-echelon alignment. See inset box to the upper right or Figure 2 for the location of the cross sections. Seismic sections courtesy of OMV cooperation.

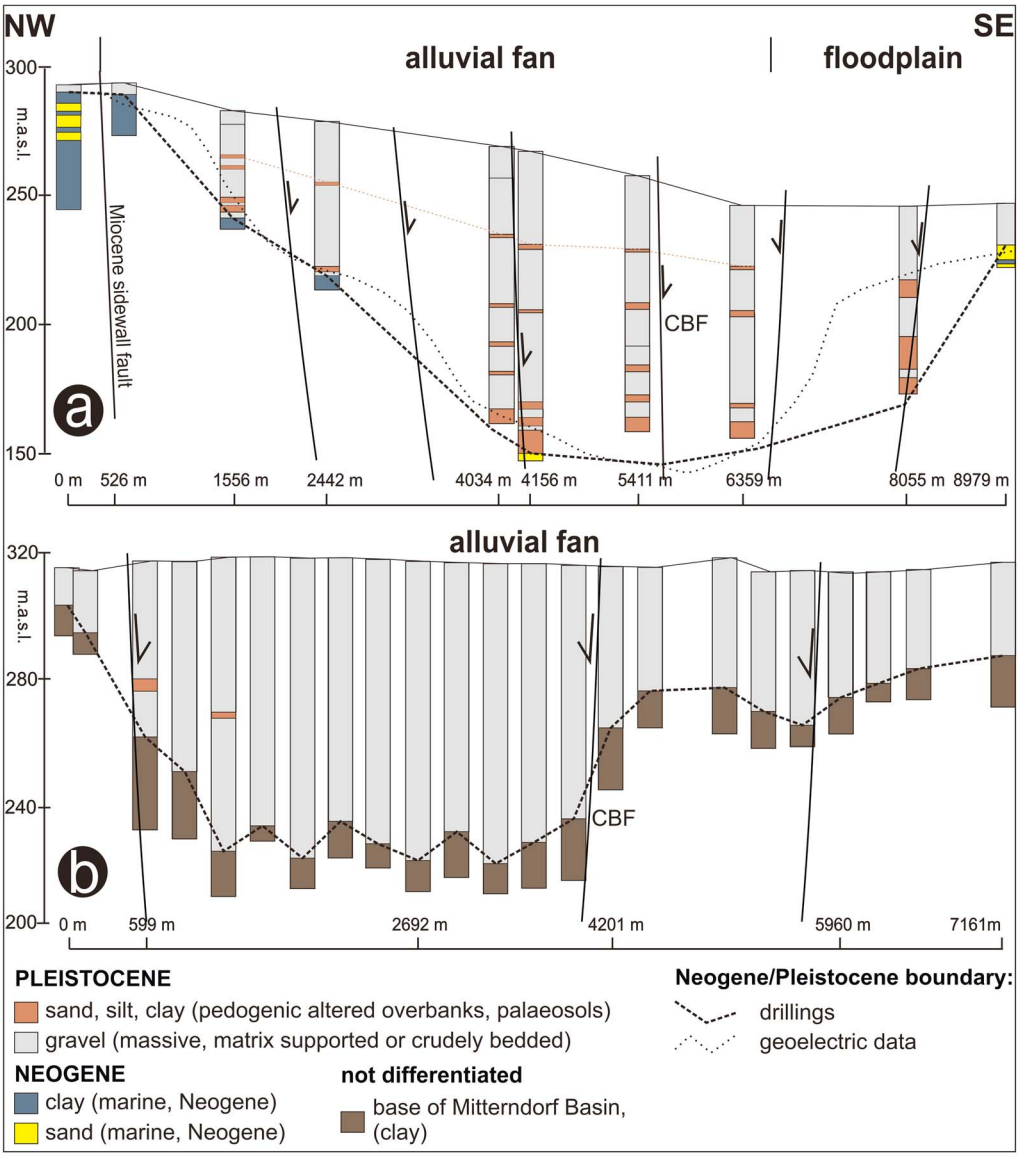

Figure 8. Cross sections through the Mitterndorf Basin with fault locations indicated by VG maxima. (a) Section is drawn based on lithologic logs of groundwater drillings with detailed information. (b) Section is drawn based on lithologic logs of closely spaced drillings (for seismic check shots) with low information content (small scale differences in lithofacies are not recorded). Thick gravel units reflect sheet flow dominance during predominantly cold periods, overbanks and paleosols reflect sedimentation during warmer periods. Geoelectric data is adapted from *Berger* [1989]. The Miocene sidewall fault (Sollenau Fault) in Figure 8a is not or only low active. CBF marks the cross-basin fault zone.

steeper the fault and the closer the structure to the surface the smaller will be the lateral separation of the VG and HG extremes and the larger will be the amplitudes. A lower fault dip produces a lower VG and HG amplitude and a longer wavelength (Figure 4, right). Similar, with increasing depth of the structure, the VG and HG signals show decreasing amplitudes and increasing wavelengths. The HG maximum remains located between the VG extremes. The large subvertical fault represented in the middle panel of Figure 4 shows higher VG, HG amplitudes, as the vertical displacement at the single fault is large. In practice, HG and VG amplitudes are smaller due to the sampling effects depending on the station interval. As VG maxima best represent the position of a fault cut off, VG anomalies and their coincidence with faults have been assessed utilizing independent data.

[22] However faulting may also be more complex. Horst-like structures or tilted blocks typical for normal fault settings, like asymmetric grabens may produce more complex maxima. In these specific cases the VG anomaly is characterized by only a single VG maximum located between two HG maxima. Such a case is typical-present in the asymmetric grabens north of the Danube (Figure 10) [cf. *Decker et al.*, 2005].

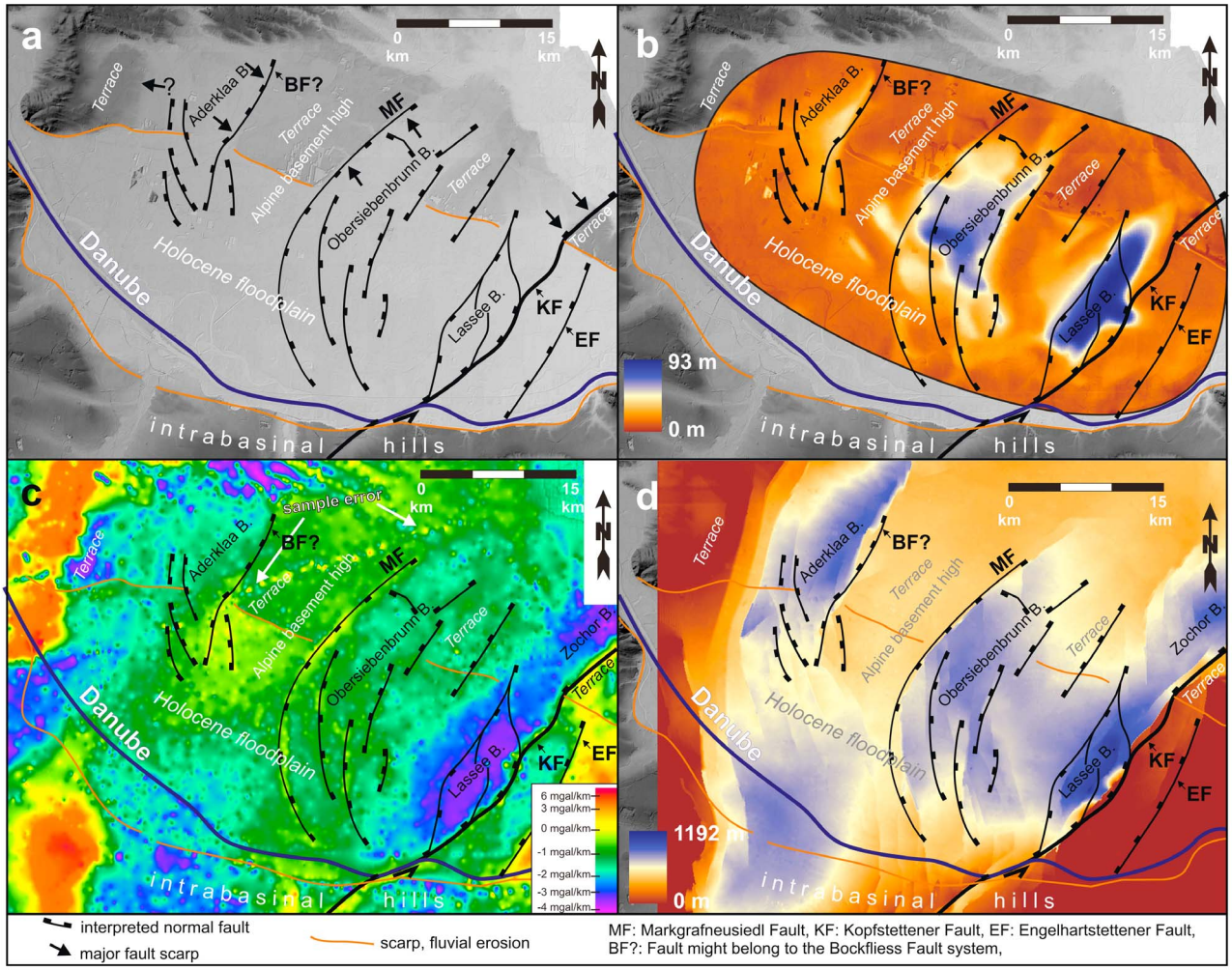

Figure 9. Pleistocene Basins and interpreted faults from VG anomalies (black) north of the Danube. (a) VG anomalies plotted on a hill-shaded DEM. Black arrows indicate fault scarps, brown lines indicate fluvial scarps. (b) Modeled thickness of Pleistocene sediments just by kriging of drillings (without fault information) [*Gangl*, 1993]. (c) VG anomalies. (d) Cumulative thickness of sediments between Top Middle Miocene (11.6 Ma [*Unterwelz*, 1993]) and surface. Drill log information was not available in the north. See text for details.

4.2. Bouguer Gravity, First-Order Derivatives and Structures

[23] The Bouguer anomaly map of the Vienna Basin shows a SW to NE elongated area with a clear gravity low of more than −40 mgal in comparison to the surrounding Alps (Figure 5a). The gravity lows in the Vienna Basin roughly coincide with the location of Pleistocene Basins and intrabasinal hills along the Danube.

[24] First-order derivatives of Bouguer data highlight near-surface structures. Occurrences of unconsolidated or low consolidated, low-density Late Miocene and Quaternary fluvial sediments (Figure 3) are represented as gravity lows in the anomaly maps: Late Miocene sediments of the Paleo-Danube especially occur along major sidewalls of the Vienna Basin [*Harzhauser et al.*, 2003] e.g., at the position of the intrabasinal hills (Figure 5b). Quaternary fluvial sediments were particularly deposited in the Mitterndorf [*Salcher et al.*, 2010] and Lassee Basin [*Beidinger et al.*, 2011]. Prominent basement highs of the Miocene Vienna Basin like the area west of the Leopoldsdorf fault and east of the Aderklaa basin [*Hamilton et al.*, 2000; *Hölzel et al.*, 2010] are associated with gravity highs. In these regions accumulation of Late Miocene and Quaternary terrestrial sediments is low or absent. VG and HG anomalies show two dominant systems in the Vienna Basin (Figure 5): (1) northeast-southwest trending maxima paralleling the VBSSF and associated Quaternary Basins and (2) short northwest-southeast trending maxima around the intrabasinal hills not exceeding 10 km in length (amplitudes of these structures are low).

4.3. The Structure of Pleistocene Pull-Apart Basins and Associated VG and HG Anomalies

[25] The Mitterndorf Basin consists of 3 depocenters (Figure 6). The largest and deepest depocenter is elongated

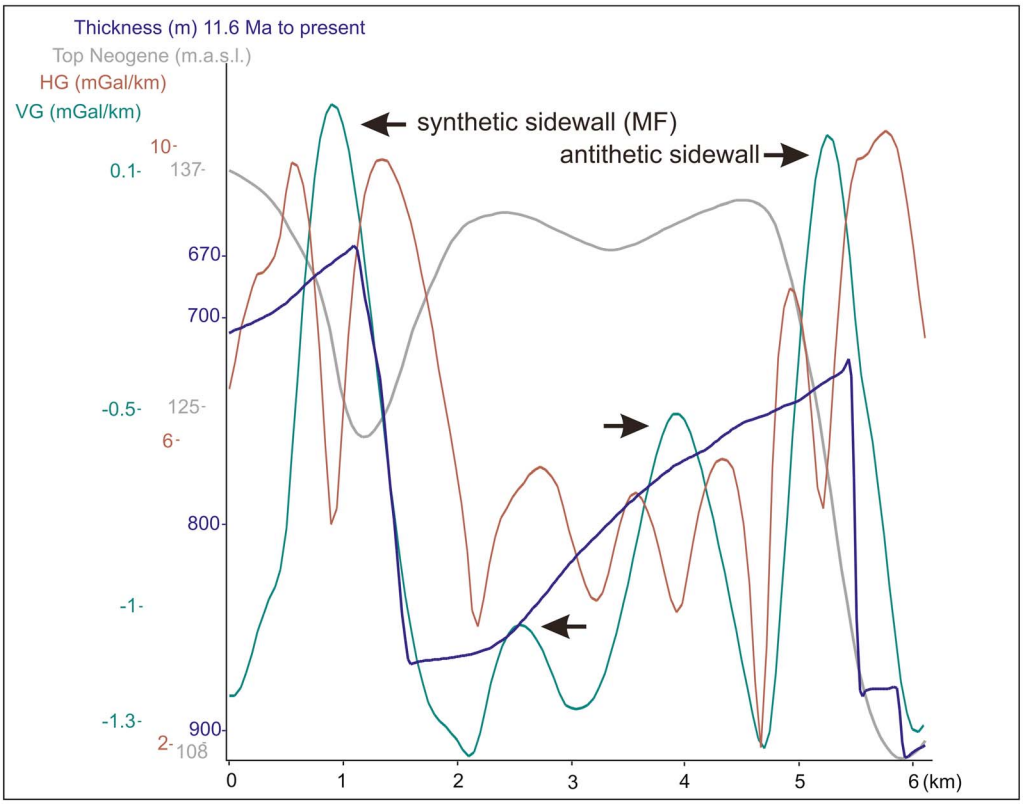

Figure 10. VG and HG profiles across the Obersiebenbrunn Basin. The locations of the profiles are shown in Figure 2. Anomalies show the response of VG (green) and HG (red) maxima to vertical displacement (normal faults). The VG maxima along the profile can be traced as faults and are marked with arrows. At 0.9 km and 3.9 km, the basement is shaped by horst-like structures associated with a VG maximum located between two HG maxima due to interference of VG/HG anomalies. The interpolated top Neogene in (gray) [*Gangl*, 1993] is contradictory to all other curves, likely due to wrong interpolation of litho facies. The blue line shows the thickness of sediments between top Middle Miocene (11.6 Ma) and surface. Highest amplitudes are related to Obersiebenbrunn Basin's the synthetic (Markgrafneusiedl fault = MF) and antithetic sidewall faults.

and situated in the northern part, reaching a maximum depth of more than 170 m. The two smaller ones are separated by a basinal high and are situated in the southern and central part of the basin reaching depths of c. 100 and 115 m, respectively. Depocenters are aligned east and west of an almost 50 km long VG anomaly maximum not wider than few hundreds of meters. This feature shows the classical position of a cross-basin fault zone [*Mann*, 2007]. In the northern, tightest part of the Mitterndorf Basin distinctly highlighted maxima represent the large vertical displacements of Pleistocene to Neogene strata. Three-dimensional [*Hinsch et al.*, 2005] and two-dimensional reflection seismic covering the northern part of the Mitterndorf Basin show that these anomalies are in a good agreement with Upper Miocene faults of the underlying negative flower structure (Figure 7a). The anomalies in the central part of the Basin are segmented in a sub-parallel, right stepping en-echelon pattern with the appearance of Riedel and anti-Riedel shears (Figure 6). In the south, anomaly maxima are curved in a terraced alignment around the depocenter and converge into the strike-slip segment of the Alpine Mur-Mürz fault.

[26] Possible fault locations in the Mitterndorf Basin can principally constrained in areas of high drill log density as the difference in lithofacies between marine Neogene and fluvial Pleistocene sediments as well as its internal built-up is very characteristic. Figure 8 shows a drill section with offset strata indicating a good fit with fault positions derived from mapped VG maxima. The available geoelectric sections covering the entire Mitterndorf Basin [*Berger*, 1989] are less appropriate to constrain fault positions due to large sampling intervals (in the order of few km) but well resolve large structures of the Pleistocene basement, i.e., basinal highs and lows (Figure 8).

[27] The Mitterndorf Basin is connected via a NE-striking, several km long, strong VG and HG maximum to the releasing bend of the Lassee Basin situated in the northeast. The VG maximum coincides with a distinct topographic depression (graben) within the intrabasinal hills (Figure 11, yellow line).

[28] Like the Mitterndorf Basin, the Lassee Basin is part of a reactivated Late Miocene negative flower structure [*Beidinger and Decker*, 2011]. A VG and HG low marks a

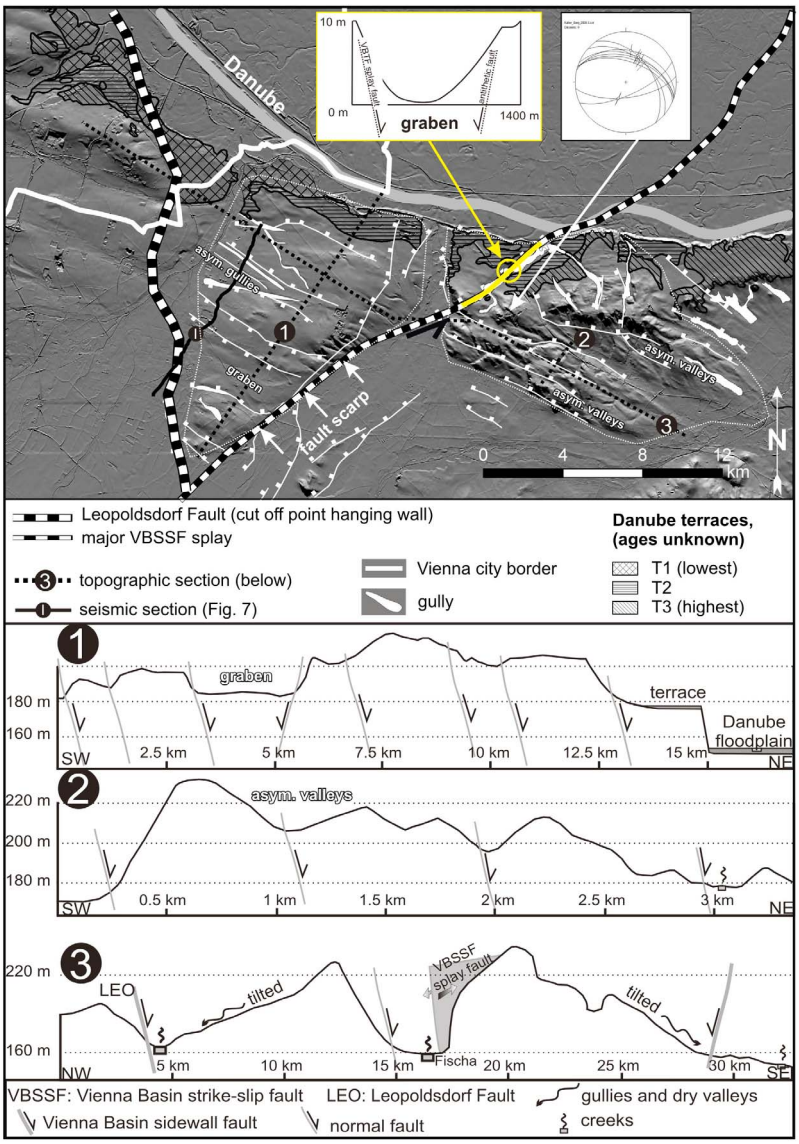

Figure 11. Tectonics and geomorphology of intrabasinal hills. Linearly, NW striking gullies, valleys and graben ridges coincide with normal faults (1 and 2). Dry valleys and gullies form along faults. Geomorphology results from faulting relating to Plio-/Pleistocene NE-SW extension of the Vienna Basin. Faulting is also evident from fault slip data (inset box; Schmidt's net lower hemisphere projection). White arrows mark a major fault scarp delimiting the intrabasinal hills to the Mitterndorf Basin. Low Pleistocene fault activity of Miocene Vienna Basin's sidewall faults caused the tilting of the hills (3). Sidewalls of the graben linking the Mitterndorf and Lassee Basin structure (yellow line and yellow outlined inset) coincide with positions of a major VBSSF branch and its antithetic fault. Terrace levels according to the geological map of Vienna and vicinity (1,200,000 [*Fuchs and Grill*, 1984]).

c. 9 km long, about 3 km wide, elongated depocenter (Figure 9c). The Lassee Basin's eastern boundary is manifested by a strong VG maximum marking high vertical offsets along branch faults (Figure 7c) of the underlying negative flower structure. Branch faults are typically very steep and closely spaced so that the VG maxima (Figure 7c; 16–18) represent multiple faults in an en-echelon alignment. These faults are associated with a scarp in the NE [*Beidinger et al.*, 2011] delimiting the basin to a Late Pleistocene terrace (Figure 9a). The entire fault branch on each side of the Lassee basin is about 1.5–2 km wide. To the west, VG anomalies continuously increase with no distinct maximum (Figure 9c) suggesting a continuous decrease in Pleistocene infilling with lower vertical offsets along faults. Basin's depocenter, however, is limited by a weak VG maximum to the west, coinciding with branch faults (Figure 7c and 9d). Faults have generally no surface expression within Danube's floodplain. In the north, the

Lassee basin is linked to the Zohor Basin (Slovakia) via a short, few kilometers long basinal high with low Pleistocene cover [*Fendek and Fendekova*, 2005] (Figure 9b). The formation of Pleistocene pull-aparts along the VBSSF continuous further with the Pernek and the Sološnica Basin at the westernmost Carpathian Foreland and terminates in the Western Carpathians with an about 100 km wide restraining bend [*Fojtíková et al.*, 2010] (Figure 1).

4.4. The Structure of Pleistocene Grabens and Associated VG and HG Anomalies

[29] A lower thickness of Late Miocene and Pleistocene fluvial deposits in the Obersiebenbrunn and Aderklaa Basin [*Bernhard et al.*, 1992; *Gangl*, 1993; *Darsow et al.*, 2009] is indicated by higher VG values compared to the Mitterndorf and Lassee Basin (Figure 9b). Basins evolve as grabens along reactivated, major listric normal faults east and west of a prominent basement high (Aderklaa high) [*Hamilton et al.*, 2000] (Figure 9). These faults built Obersiebenbrunn and Aderklaa Basin's synthetic faults and form prominent fault scarps in terrace deposits outside Danube's floodplain [*Decker et al.*, 2005] (Figure 9a). Similar to the Lassee Basin, distinct VG and HG maxima (Figure 10) indicate normal faulting far into the floodplain, which is evident by the Quaternary basin infill (Figure 9b). Holocene activity of synthetic sidewall faults is proven by faulted sediments [*Chwatal et al.*, 2005; *Hintersberger et al.*, 2011]. Historical seismicity, however, is low [*Grünthal et al.*, 2009].

[30] Obersiebenbrunn Basin's synthetic faults are curved, turning from NE into NW direction toward the VBSSF were they are supposed to splay off [*Decker et al.*, 2005]. The absence of distinct VG or HG maxima close to the VBSSF indicates decreasing vertical displacements toward the intersection. The basin's largest sidewall (MF, Figures 7c, 9c, and 10) has a high relevance for Vienna Basins' formation processes throughout the Miocene and Quaternary. The VG and HG maximum runs parallel to the pre-Neogene basement and Top Middle Miocene cut off line for more than 20 km, vertically offsetting the basement up to 600 m [*Kröll and Wessely*, 1993] and the Top Middle Miocene up to 300 m [*Unterwelz*, 1993] (Figure 9d). Density differences between basement's and Middle Miocene's hanging and footwall in a minimum depth of c. –3100 m and c. –600 m respectively do not influence VG and HG maxima.

[31] In contrast to the Obersiebenbrunn basin, Aderklaa basin's faults are not linked to the VBSSF. This is indicated by mapped VG anomalies not converging toward the VBSSF as well as the Miocene and Quaternary isopach maps. However, the reconstructed distribution of the Quaternary infill [*Gangl*, 1993; *Darsow et al.*, 2009] (Figure 9b) does only partly fit the Miocene isopach map and suggested faults from VG maxima (Figures 9d and 10). The lack of precise log data from deeper sections and the resulting inaccurate interpolation might be the reason for the deviation.

4.5. The Major Leopoldsdorf Fault System and Associated VG and HG Anomalies

[32] Short VG and HG maxima associated with faulted Pleistocene basins differ from long wavelength maxima associated with Miocene sidewalls of the Vienna Basin with a lower dip and very high vertical displacements, i.e., the Leopoldsdorf fault system (Figure 5). Miocene sidewalls displace Alpine rocks close to the surface with a high density difference to the Miocene sedimentary hanging wall. The situation of a low dipping normal fault has been modeled in Figure 4 (right) and is typically associated with a wide wavelength VG/HG maximum and a large horizontal offset of the HG in relation to the VG. The Leopoldsdorf fault systems as one of Vienna Basin's largest structures, displaces the Miocene sediments from an intrabasinal high of pre-Neogene (Alpine) basement rocks (c. −120 m to several 1000 m with sets of comparably low dipping normal faults (mean $\sim 50°$) (Figure 7b). The VG maximum coincides with the westernmost and largest normal fault of the system displacing Alpine rocks to c. −2400 m [*Wessely*, 1979]. The maximum of the HG has a c. 2.5 km offset to the maximum of the VG in the west (Figures 5b and 5c).

4.6. Intrabasinal Hills, VG and HG Anomalies and Geomorphic Features

[33] An up to 50 m high erosional escarpment separates the Danube's floodplain from a chain of hills marking the most striking elevations crossing the Vienna Basin (Figure 11). Tilting of the hills (Figure 11, section 3) is related to the very low activity of Vienna Basin's Miocene sidewalls (Leopoldsdorf fault in the west and Engelhartstettener fault in the east; Figure 5). It is not clear whether activity was continuously low since the Late Miocene, or minor reactivation occurred later. Intrabasinal hills are associated with generally low VG and HG values (Figure 5b). Accurate log information of the top tens of meters is sparse, showing the regular alternation of c. 10 m thick units of gravels and clayey sediments with a total thickness of c. 60 m. These sediments are sometimes unconformably overlain by several meters thick Pleistocene fluvial gravels of the Danube [*Fink and Majdan*, 1954]. Alternating sequences are interpreted as cyclic deltaic deposits of the Late Miocene Danube and Paratethyian sea [*Salcher*, 2008]. Outcrops show that compaction of fluvial sediments is typically low (Figure 3), likely to cause the strong VG and HG deficit in the area of the intrabasinal hills. A gravity high coinciding with a topographic N-S striking valley structure separates the hills indicating the complete erosion of low-density deltaic sediments through a Danube tributary (Figure 11, section 3). Drill logs, which document predominantly clayey to fine sandy marine deposits, corroborate that assumption. A further strong, linear NE-SW striking anomaly maximum coincides with a graben structure forming as a consequence of normal faulting along a major VBSSF splay and its antithetic faults (Figure 11, inset sketch).

[34] Generally weaker maxima coincide with NW-SE striking geomorphic features. Features include sub-parallel striking grabens, asymmetric discontinuous (dry) valleys and gullies (Figure 11, sections 1 and 2). Industrial reflection seismic (Figure 7b) and field analyses (Figure 11, inset Schmidt net) demonstrate that these features are related to sets of conjugated normal faults developing between Vienna Basin's Miocene sidewalls. Seismic data show that the vertical displacements of these structures are commonly not more than 15 m (Figure 7b). The internal built up of the hills (especially at the top 100 m) is not well documented; comprehensive data on hanging and footwall density is not

available. Statements on the nature of these maxima remain therefore vague.

5. Discussion

[35] So far, detailed studies on Quaternary faulting of the Vienna Basin mainly base on deformation data of Miocene strata and modern topography [*Hinsch et al.*, 2005; *Beidinger and Decker*, 2011]. Information on structures is accurate but locally limited to existing 3-D and 2-D seismic surveys, which do not cover the top hundreds of meters. The utilization of gravity derivatives in combination with common geological and geophysical methods significantly reduced the lack of fault trace information. The presented structural model gives the so far most precise and complete picture of the recent kinematics of the Vienna Basin.

5.1. The Reactivation of Miocene Structures During the Quaternary

[36] Reliable statements on fault reactivation are possible were independent data from both, Miocene and Quaternary strata are available (Figures 6 and 8). This is especially true for the northern part of the Mitterndorf Basin, which is covered by a 3-D seismic cube [*Hinsch et al.*, 2005] and several hundreds of drill logs (Figure 6). *Unterwelz* [1993] presented the most accurate map for the Late Miocene structure of the central part of the Vienna Basin (Figure 9d and Table 1). Structural information is based on drillings and on a dense network of relatively low resolution seismic sections (based on surveys from the 60s and 70s). VG maxima indicate a good coincidence with Late Miocene normal faults, but in the absence of precise stratigraphic data, statements on the (re-) activation of some individual faults remain vague. However, basin fill and data from topography and recent field analysis [e.g., *Chwatal et al.*, 2005; *Hintersberger et al.*, 2011] proof that at least the large basin sidewalls have been reactivated during the Quaternary (Figure 9).

[37] From the inspection of the data, it is obvious that the structural model of the Vienna Basin's Alpine basement lack high resolution information, showing only large faults or fault zones [*Kröll and Wessely*, 1993]. Even though basin kinematics largely changed during the Miocene [*Decker and Peresson*, 1996] data indicate that especially faults or fault zones in the east of the basin have been active during the Quaternary (e.g., Markgrafneusiedl Fault, Kopfstettener Fault or Bockfliess Fault system, Figure 5). This is not surprising as the Late Miocene and Quaternary subsidence is focused on the side of the basin [*Jiřiček and Seifert*, 1990]. In contrast, the major Middle Miocene sidewalls in the western part are very low active (Steinberg Fault and Leopoldsdorf Fault; Figures 5 and 11) or inactive (Sollenau Fault; Figures 5 and 8a).

5.2. Tectonics of Pleistocene Basins

[38] Steeply dipping, sub-vertical faults dominate Pleistocene basins. They show distinct VG, HG maxima associated with short wavelengths (Figure 5). HG and VG maxima appear often superimposed.

[39] The compiled structural map (Figure 6) indicates that the Mitterndorf basin did not develop due to pure strike-slip motion between the offset PDZs but rather with some degrees offset. En-echelon sidewall faulting, the development of a cross-basin fault delimiting opposite depocenters are characteristic features of pull-apart basins in a transtensional setting [*Wakabayashi et al.*, 2004; *Mann*, 2007; *Wakabayashi*, 2007] (Figure 12). En-echelon basin sidewalls are interpreted as reactivated Riedel (R) and anti-Riedel (R′) fractures [*Smit et al.*, 2008, 2010] (Figure 6), typically inducing relay ramps (R) [e.g., *Schlische et al.*, 2002; *Frankowicz and McClay*, 2010]. The almost 50 km long VG anomaly maximum delimiting basin's depocenters on each side is interpreted as a cross-basin fault zone. Cross-basin fault zones form as consequence of strain partitioning between offset PDZs in transtensional strike-slip settings [*Smit et al.*, 2008, 2010]. Analog models show that fault segments of cross-basin fault systems develop as tight, steeply dipping segments in an en-echelon pattern flipping longitudinally across the basin [*Wu et al.*, 2009]. Flipping around depocenters is evident in the Mitterndorf Basin; differentiation of steeply dipping segments is not possible as segments appear as single VG maximum.

[40] The impact of active faulting along the Mitterndorf Basin is shown by an approximately 60 m high fault scarp delimiting Late Miocene from Holocene strata in the north [*Hinsch et al.*, 2005] (Figure 6). This fault is associated with moderate seismicity with a historical M_{max} = 5.2 (I_0 = 8) earthquake (Central Institute for Meteorology and Geodynamics, Catalogue of earthquakes in Austria 1201–2008, computer file, 2008). Higher subsidence rates in the north are not only demonstrated by a higher sediment thickness but also in the formation of a sag pond [*Decker et al.*, 2005] resulting in extensive occurrences of flood and peat deposits [*Havinga*, 1972] (Figures 6 and 12), evident from driller's lithologic logs. Given an age of 250–300 ka for the Mitterndorf Basin [*Salcher*, 2008] the average subsidence rate of the northern, deepest part corresponds to c. 0.6–0.7 mm/a. Interestingly, this value is very similar to the mean Miocene subsidence rate of Vienna Basin's largest and deepest depocenter (5.8 km Miocene sediments; [*Sauer et al.*, 1992]).

[41] The c. 4.5 km long, narrow graben structure liking the Mitterndorf and Lassee strike-slip basin (Figure 11, yellow line) may appear as classical feature of transtensional pull-apart basins where such narrow grabens typically form in inline above the PDZs [*Garfunkel and Ben-Avraham*, 1996; *Wu et al.*, 2009]. However, as shown in reflection seismic, the position of VBSSF's PDZ does not coincide with this graben [*Hinsch et al.*, 2005; *Beidinger and Decker*, 2011]. The graben develops along an east dipping major splay of the negative flower structure and its associated antithetic faults (Figure 11, inset sketch). This major splay is likely to merge with Lassee basin's eastern sidewalls, which have the opposite dip.

[42] The eastward growth thickness of sediment in the Lassee basin is associated with a continuous decrease of VG and HG values (Figure 9c) reflecting a strong basin asymmetry (Figure 7c). This also indicated in the sidewall fault geometry of the basin: In contrast to the western sidewalls, eastern sidewalls are very closely spaced (Figure 12), [*Beidinger and Decker*, 2011]. Low, gradual displacements of the western sidewalls do not enforce a strong gravity signal. In contrast, eastern sidewalls have high vertical displacements along tightly spaced faults that appear as a single anomaly maximum. The large vertical displacements

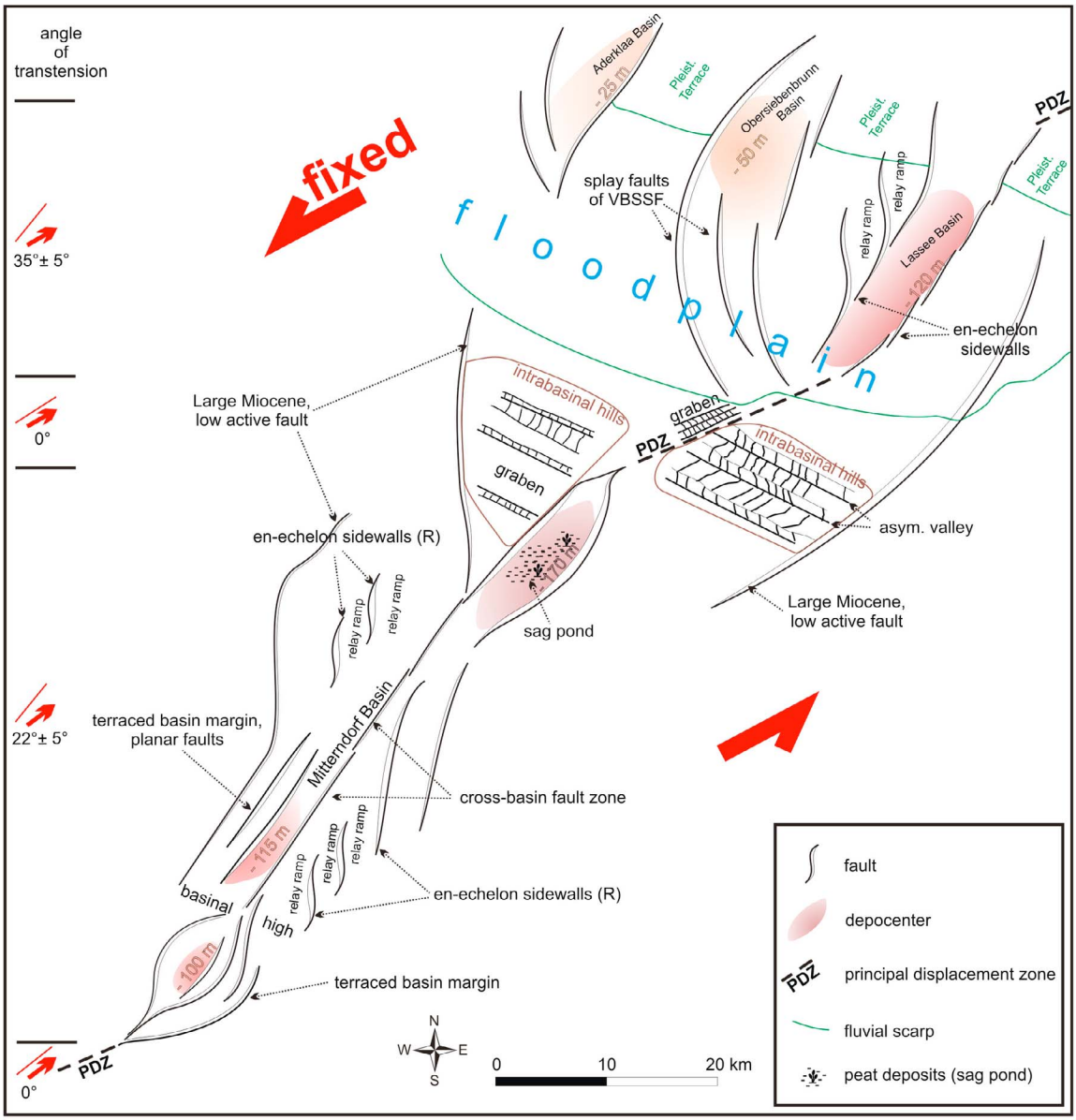

Figure 12. Idealized and simplified structural map of the Quaternary Vienna Basin. The Mitterndorf Basin shows classical features of a pull-apart in transtension like the formation of cross-a basin fault zone and en-echelon basin margins. The high transtensional angle in the Lassee Basin caused very asymmetric sidewall faulting. Obersiebenbrunn Basin develops along splays of the VBSSF and its antithetic faults. Transtensional angle according to *Beidinger and Decker* [2011] and *Grenerczy et al.* [2000]. Vertical offset of faults is indicated but not to scale. See text for details.

produce high amplitudes because faults delimit a thick pile of relatively low-density Pleistocene sediments from dense Alpine rocks close to the surface where Neogene and Quaternary cover is minor (Figures 9b and 9d). Given the sensitivity of pull-aparts to even very low transtensional angles (the angle between the PDZ and the crustal movement vector) leading into different features [*Mann et al.*, 1983; *Smit et al.*, 2008, 2010], the extreme asymmetry in sidewall faulting rather gives the Lassee basin the impression of a half-graben structure. The transtensional angle of the Mitterndorf Basin and the main strike-slip fault is much smaller [*Hinsch et al.*, 2005], which therefore resembles more a pull-apart basin, even though very differently sized depocenters might also refer to asymmetry [*Wu et al.*, 2009]. The transtensional angle inferred for the Lassee basin is c. 35° and only c. 22° for the Mitterndorf basin [*Beidinger and Decker*, 2011]. It has been reported that the relatively longitudinal symmetry developing in pull-apart basins resulted from the equal rate of strike-slip displacement [*Wu et al.*, 2009]. Longitudinally asymmetric pull-apart basins would be expected when the opposing sides of the basin move with unequal rates of strike-slip motion [*Rahe et al.*, 1998; *Basile and Brun*, 1999], or with only one moving plate [*Rahe et al.*, 1998; *Smit et al.*, 2008]. Movement along

the VBSSF is entirely related to the crustal block to the east (Figure 1) ("Styrian-West Carpathian Wedge" [*Decker et al.*, 2005]). Aside from the transtensional angle, single block movement might therefore also contribute to the asymmetry of the pull-aparts.

[43] The area between the Lassee and Mitterndorf Basin is suggested to act as major kinematic boundary [*Hinsch et al.*, 2005; *Hinsch and Decker*, 2011]. The transtensional angle of this segment connecting both basins is almost zero, causing only weak opening of the linking graben structure (Figure 11, yellow line) which parallels the PDZ. The increased extension north of the Danube is reflected by a higher transtensional angle and interpreted to be additionally accommodated by faults related to the Obersiebenbrunn and Aderklaa Basin [*Beidinger and Decker*, 2011]. Graben formation along these faults can therefore be regarded as the result of strain partitioning along the VBSSF [*Hinsch et al.*, 2005]. Splay faulting similar to the fault sets related to the Obersiebenbrunn basin are reported from other natural strike-slip systems (e.g., Dead Sea Basin) and analogue models of pull-apart basins [e.g., *Smit et al.*, 2008], where outer basin faults nucleate at the lateral edge of the basal décollement layer [*Wu et al.*, 2009].

5.3. Tectonic Geomorphology of Intrabasinal Hills

[44] Ongoing uplift of the Vienna Basin and its vicinity since the Pliocene caused incision of the Danube and all of its tributaries, leaving the hills as erosional remnants well preserving tectonic activity. Our data indicates that NW-striking grabens and asymmetric valleys are young fault-controlled morphologies (Figure 11, sections 1 and 2). As no sedimentary growth is associated with faulting, structures manifested in NW-SE striking VG and HG maxima are interpreted as younger than Late Miocene. This assumption is corroborated by soil stratigraphy of graben infillings in adjacent regions. Fillings are roughly constrained to Pliocene to Pleistocene. These NW- striking geomorphologic features are not only pronounced within the Vienna Basin, but also in the adjacent Alpine Molasse [e.g., *Havlicek et al.*, 1998], the Bohemian Massive [e.g., *Roštínský et al.*, 2005], the Pannonian Basin [e.g., *Zámolyi et al.*, 2010], the Alps [e.g., *Wessely*, 2006] and the Western Carpathians [e.g., *Wessely*, 1961; *Kováč et al.*, 2002]. The cause for these structures is not clear but might have a superregional origin. NW - SE faulting is one of the most prevalent directions in the European continental crust, since at least Permian times and shown to be reactivated at multiple times [e.g., *Genser et al.*, 2007].

5.4. Limitations

[45] VG and HG signals may also highlight structures that are not normal fault related (e.g., the Alpine mountain front) or represent complex structures with VG and HG signals are more difficult to interpret (like horsts and grabens, Figure 10). Therefore, maxima related to faults or a fault zone should generally only be assessed where other independent data sets are available (e.g., drill logs or reflexion seismic). Furthermore, anomalies can be locally superimposed by positive or negative, isolated short-wavelength features. Hence, maxima must be present over larger horizontal distances (here more than 2 km). Fault reactivation timing can only be reliably made if sediment growth or fault rupturing is evident in sediments of known age (Figures 6, 8, and 9) [cf. *Hinsch et al.*, 2005]. VG maxima may not always represent a single fault but also a set of normal faults. The reactivated eastern sidewall of the Lassee Basin, for example, is represented by very closely spaced faults [*Beidinger and Decker*, 2011] but appears as a single strong VG maximum (Figure 9).

6. Conclusions

[46] High pass characteristic of Bouguer's first-order gravity derivatives (VG and HG) were found to suitably detect near-surface structures in the Vienna Basin and successfully compensated the lack of fault information. Faults anomalies produce a VG maximum close to the footwall cut off and a minimum close to the hanging wall cut off, the HG maximum is situated in between. Aside from the density difference between the hanging wall and footwall, structure depth, fault dip angle and vertical displacement largely influence the signals: the higher the dip angle, the longer the wavelength and the deeper the structure, the lower is the amplitude. The accumulation of terrestrial Quaternary and Late Miocene sediments produce significant VG and HG gravity lows in reactivated basins and along major sidewalls of the Vienna Basin. Geometries of Quaternary basins, which form as consequence of sinistral movement along the VBSSF, have been identified by the integration of geological and geophysical data highlighting pull-aparts and tectonic grabens. Pull-aparts develop as transtensional basins, with high angles between the offsets PDZs and the movement vector of the moving plate east of the VBSSF. The Mitterndorf Basin, south of the Danube, forms with a transtensional angle of around 20° and develops still classical features of a transtensional pull-apart such as a cross basin fault delimiting opposite depocenters and en-echelon sidewalls with intervening relay ramps. North of the Danube a larger extension resulted in a higher transtensional angle of the Lassee pull-apart and is additionally compensated by the opening of two graben systems. The Lassee-pull-apart shows an extreme asymmetry, which results in the absence of separated depocenters and a very different sidewall fault geometry. Faults of Quaternary Basins largely resemble preexisting structures of the Late Miocene, which were reactivated during the Late Middle Pleistocene. Further active systems in the Vienna Basin are associated with short NW-SE striking geomorphic features and the tilting of hills along major Miocene sidewalls. Both systems have low activity. NW-SE faulting has likely started in the Pliocene or Early Pleistocene and represents continental scale stresses.

[47] **Acknowledgments.** Bouguer Gravity, reflection seismic, hydrocarbon drilling, and rock density database courtesy of OMV cooperation. Additional gravity data courtesy of Federal Office of Metrology and Surveying. The hydrological drilling database and the digital terrain model were provided by the Geological Survey of Austria and Government of Lower Austria, respectively. Robert Faber, TerraMath (www.terramath.com), provided the code for inverse distance modeling. The work was supported by the Austria Science Foundation (FWF) and the European Science Foundation (ESF). We further acknowledge fruitful discussions with Andreas Beidinger (basin kinematics, seismic data), Mathias Harzhauser (Late Miocene stratigraphy), Wolfgang Lenhardt (earthquake data), and Godfrid Wessely (structure and tectonics of the overall Vienna Basin). Rebecca Reverman is acknowledged for a thoughtful and thorough reading of the manuscript. We are grateful to Frank Horvath, Miroslav Bielik, and an anonymous reviewer who provided constructive and insightful reviews.

References

Achmon, M., and Z. Ben-Avraham (1997), The deep structure of the Carmel fault zone, northern Israel, from gravity field analysis, *Tectonics*, *16*, 563–569, doi:10.1029/96TC02912.

Basile, C., and J. P. Brun (1999), Transtensional faulting patterns ranging from pull apart basins to transform continental margins; an experimental investigation, *J. Struct. Geol.*, *21*, 23–37, doi:10.1016/S0191-8141(98)00094-7.

Beidinger, A., and K. Decker (2011), 3D geometry and kinematics of the Lassee flower structure: Implications for segmentation and seismotectonics of the Vienna Basin strike-slip fault, Austria, *Tectonophysics*, *499*, 22–40, doi:10.1016/j.tecto.2010.11.006.

Beidinger, A., K. Decker, and K. H. Roch (2011), The Lassee Segment of the Vienna Basin Fault System as a potential source of the earthquake of Carnuntum in the 4th century A.D, *Int. J. Earth Sci.*, *100*, 1315–1329, doi:10.1007/s00531-010-0546-x.

Ben-Avraham, Z., U. Brink, R. Bell, and M. Reznikov (1996), Gravity field over the Sea of Galilee: Evidence for a composite basin along a transform fault, *J. Geophys. Res.*, *101*, 533–544, doi:10.1029/95JB03043.

Berger, E. (1989), Analyse der Funktionsfaktoren des Grundwasserspeichers Mitterndorfer Senke, scientific report, Amt der NÖ Landesregierung, Vienna.

Bernhard, M., E. Niesner, and B. Holub (1992), Geophysikalisch-hydrologische Untersuchungen jungtertärer Tiefensüßwasser im Raum Wien: Teil A, scientific report, 112 pp., Montanuniv. Leoben, Vienna.

Blakely, R. (1995), *Potential Theory in Gravity and Magnetic Applications*, 441 pp., Cambridge Univ. Press, Cambridge, U. K., doi:10.1017/CBO9780511549816.

Bott, M. H. P. (1962), A simple criterion for interpreting negative gravity anomalies, *Geophysics*, *27*, 376–381, doi:10.1190/1.1439026.

Brix, F., and O. Schulz (Eds.) (1993), *Erdöl und Erdgas in Österreich*, 688 pp., Mus. of Nat. Hist., Vienna.

Brückl, E., M. Behm, K. Decker, M. Grad, A. Guterch, G. R. Keller, and H. Thybo (2010), Crustal structure and active tectonics in the Eastern Alps, *Tectonics*, *29*, TC2011, doi:10.1029/2009TC002491.

Büyüksaraç, A., D. Jordanova, A. Ateş, and V. Karloukovski (2005), Interpretation of the gravity and magnetic anomalies of the Cappadocia region, central Turkey, *Pure Appl. Geophys.*, *162*, 2197–2213, doi:10.1007/s00024-005-2712-9.

Chwatal, W., K. Decker, and K. H. Roch (2005), Mapping of active capable faults by high-resolution geophysical methods: Examples from the central Vienna Basin, *Austrian J. Earth Sci.*, *97*, 52–59.

Csontos, L., A. Nagymarosy, F. Horváth, and M. Kovác (1992), Tertiary evolution of the Intra-Carpathian area: A model, *Tectonophysics*, *208*, 221–241, doi:10.1016/0040-1951(92)90346-8.

Darsow, A., M. T. Schafmeister, and T. Hofmann (2009), An ArcGis approach to include tectonic structures in point data regionalization, *Ground Water*, *47*, 591–597, doi:10.1111/j.1745-6584.2009.00546.x.

Decker, K. (1996), Miocene tectonics at the Alpine-Carpathian junction and the evolution of the Vienna Basin, *Mitt. Ges. Geol. Bergbaustud. Oesterr.*, *41*, 33–44.

Decker, K., and H. Peresson (1996), Tertiary kinematics in the Alpine Carpathian-Pannonian system. Links between thrusting, transform faulting and crustal extension, in *Oil and Gas in Alpidic Thrustbelts and Basins of Central and Eastern Europe*, *EAGE Spec. Publ.*, vol. 5, edited by G. Wessely and W. Liebl, pp. 69–77, Geol. Soc., London.

Decker, K., H. Peresson, and R. Hinsch (2005), Active tectonics and Quaternary basin formation along the Vienna Basin Transform fault, *Quat. Sci. Rev.*, *24*, 305–320, doi:10.1016/j.quascirev.2004.04.012.

Fendek, M., and M. Fendekova (2005), Transboundary flow modeling: The Zohor Depression of Austria and the Slovak Republic, *Ground Water*, *43*, 717–721, doi:10.1111/j.1745-6584.2005.00102.x.

Fink, J., and H. Majdan (1954), Zur Gliederung der pleistozänen Terrassen des Wiener Raumes, *Jahrb. Geol. Bundesanst.*, *97*, 211–249.

Fodor, L. (1995), From transpression to transtension, Oligiocene-Miocene structural evolution in the Vienna Basin and the East Alpine-Western Carpathian junction, *Tectonophysics*, *242*, 151–182, doi:10.1016/0040-1951(94)00158-6.

Fojtíková, L., V. Vavryčuk, A. Cipicar, and J. Madrás (2010), Focal mechanism of micro-earthquakes in the Dobrá Voda seismoactive area in the Malé Karpaty Mts. (Little Carpathians), Slovakia, *Tectonophysics*, *492*, 213–229, doi:10.1016/j.tecto.2010.06.007.

Frankowicz, E., and K. R. McClay (2010), Extensional fault segmentation and linkages, Bonaparte Basin, outer West Shelf, Australia, *AAPG Bull.*, *94*, 977–1010, doi:10.1306/01051009120.

Fuchs, R., and W. Hamilton (2006), New depositional architecture for an old giant: The Matzen Field, Austria, in *The Carpathians and Their Foreland: Geology and Hydrocarbon Resources*, edited by J. Golonka and F. J. Picha, *AAPG Mem.*, *84*, 205–219, doi:10.1306/985609M843069.

Fuchs, W., and R. Grill (1984), Geological map of Vienna and its surroundings, Austrian Geol. Surv., Vienna.

Gangl, G. (1993), Die geologischen Vorerkundungen und die Grundwasserverhältnisse beim Donaukraftwerk Freudenau Teil I, Geologische Vorarbeiten für das Donaukraftwerk Freudenau am Stadtrand von Wien, *Mitt. Inst. Bodenforsch. Baugeol., Abt. Baugeol., Reihe Angew. Geowiss.*, *3*, 55–68.

Garfunkel, Z., and Z. Ben-Avraham (1996), The structure of the Dead Sea basin, *Tectonophysics*, *266*, 155–176, doi:10.1016/S0040-1951(96)00188-6.

Genser, J., S. A. P. L. Cloetingh, and F. Neubauer (2007), Late orogenic rebound and oblique Alpine convergence: New constraints from subsidence analysis of the Austrian Molasse Basin, *Global Planet. Change*, *58*, 214–223, doi:10.1016/j.gloplacha.2007.03.010.

Granser, H. (1987), Three-dimensional interpretation of gravity data from sedimentary basins using an exponential density-depth function, *Geophys. Prospect.*, *35*, 1030–1041, doi:10.1111/j.1365-2478.1987.tb00858.x.

Grenerczy, G., A. Kenyeres, and I. Fejes (2000), Present crustal movement and strain distribution in Central Europe inferred from GPS measurements, *J. Geophys. Res.*, *105*, 21,835–21,846, doi:10.1029/2000JB900127.

Grenerczy, G., A. Kenyeres, and I. Fejes (2006), Crustal deformation between Adria and the European platform from space geodesy, in *The Adria Microplate: GPS Geodesy, Tectonics and Hazards*, *NATO Sci. Ser. IV*, vol. 61, pp. 321–334, edited by N. Pinter et al., Springer, Dordrecht, doi:10.1007/1-4020-4235-3_22.

Grünthal, G., R. Wahlström, and D. Stromeyer (2009), The unified catalogue of earthquakes in central, northern and northwestern Europe (CENEC)–updated and expanded to the last millennium (2009), *J. Seismol.*, *13*, 517–541, doi:10.1007/s10950-008-9144-9.

Gutdeutsch, R., and K. Aric (1988), Seismicity and neotectonics of the East Alpine-Carpathian and Pannonian Aera, *AAPG Mem.*, *45*, 183–194.

Hamilton, W., L. Wagner, and G. Wessely (2000), Oil and gas in Austria, *Mitt. Oesterr. Geol. Ges.*, *92*, 235–262.

Harzhauser, M., and P. M. Tempfer (2004), Late Pannonian wetland ecology of the Vienna Basin based on the molluscs and lower vertebrate assemblages (Late Miocene, MN 9, Austria), *Cour. Forschungsinst. Senckenberg*, *246*, 55–68.

Harzhauser, M., J. Kovar-Eder, S. Nehyba, M. Ströbitzer-Hermann, J. Schwarz, J. Wójcicki, and I. Zorn (2003), An early Pannonian (Late Miocene) transgression in the northern Vienna Basin. The Paleoecological feedback, *Geol. Carpathica*, *54*, 41–52.

Harzhauser, M., G. Daxner-Höck, and W. E. Piller (2004), An integrated stratigraphy of the Pannonian (Late Miocene) in the Vienna Basin, *Austrian J. Earth Sci.*, *95/96*, 6–19.

Havinga, A. J. (1972), A palynological investigation in the Pannonian climate region of Lower Austria, *Rev. Palaeobot. Palynol.*, *14*, 319–352, doi:10.1016/0034-6667(72)90025-5.

Havlicek, P., O. Holásek, L. Smoliková, and R. Roetzel (1998), Zur Entwicklung der Quartärsedimente am Südostrand der Böhmischen Masse in Niederösterreich, *Jahrb. Geol. Bundesanst.*, *41*, 51–71.

Hinsch, R., and K. Decker (2011), Seismic slip rates, potential subsurface rupture areas and seismic slip potential of the Vienna Basin Transfer Fault, *Int. J. Earth Sci.*, *100*, 1925–1935, doi:10.1007/s00531-010-0613-3.

Hinsch, R., K. Decker, and M. Wagreich (2005), 3-D mapping of segmented active faults in the southern Vienna Basin, *Quat. Sci. Rev.*, *24*, 321–336, doi:10.1016/j.quascirev.2004.04.011.

Hintersberger, E., K. Decker, and J. Lomax (2011), The extended (paleo) seismological story of the Vienna Basin, including the largest earthquake north of the Alps, *Seismol. Res. Lett.*, *82*, 301.

Höggerl, N. (1980), Repeated levelling and vertical crustal movements, problems and results, *Rock Mech. Suppl.*, *9*, 201–212.

Hölzel, M., M. Wagreich, R. Faber, and P. Strauss (2008), Regional subsidence analysis in the Vienna Basin (Austria), *Austrian J. Earth Sci.*, *101*, 88–98.

Hölzel, M., K. Decker, A. Zámolyi, P. Strauss, and M. Wagreich (2010), Lower Miocene structural evolution of the central Vienna Basin (Austria), *Mar. Pet. Geol.*, *27*, 666–681, doi:10.1016/j.marpetgeo.2009.10.005.

Horváth, F. (1993), Towards a mechanical model for the formation of the Pannonian Basin, *Tectonophysics*, *226*, 333–357, doi:10.1016/0040-1951(93)90126-5.

Jiřiček, R., and P. Seifert (1990), Paleogeography of the Neogene in the Vienna Basin and the adjacent part of the foredeep, in *Thirty Years of Geological Cooperation Between Austria and Czechoslovakia*, edited by D. Minařová and H. Lobitzer, pp. 89–105, Geol. Surv. of Austria, Vienna.

Jung, K. (1961), *Schwerkraftverfahren in der angewandten Geophysik*, 348 pp., Akad. Verlagsges. Geest und Portig, Leipzig, Germany.

Kováč, M., M. Bielik, J. Hók, P. Kováč, B. Kronome, P. Labák, P. Moczo, D. Plašienka, J. Šefara, and M. Šujan (2002), Seismic activity

and neotectonic evolution of the Western Carpathians (Slovakia), in *Neotectonics and Surface Processes: The Pannonian Basin and Alpine/ Carpathian System*, *Stephan Mueller Spec. Publ. Ser.*, vol. 3, edited by S. A. P. L. Cloetingh et al., pp. 164–184, Eur. Geopsci. Union, Munich, Germany.

Kröll, A., and G. Wessely (1993), Structural Map of the tertiary basin fill, in *Wiener Becken und angrenzende Gebiete*, edited by A. Kröll et al., Geol. Surv. of Austria, Vienna.

Lefort, J. P., and B. N. P. Agarwal (1996), Gravity evidence for an alpine buckling of the crust beneath the Paris Basin, *Tectonophysics*, *258*, 1–14, doi:10.1016/0040-1951(95)00148-4.

Linzer, H. G., K. Decker, H. Peresson, R. Dell'Mour, and W. Frisch (2002), Balancing lateral orogenic float of the Eastern Alps, *Tectonophysics*, *354*, 211–237, doi:10.1016/S0040-1951(02)00337-2.

Lopes Cardozo, G. G. O., J. B. Edel, and M. Granet (2005), Detection of active crustal structures in the Upper Rhine Graben using local earthquake tomography, gravimetry and reflection seismics, *Quat. Sci. Rev.*, *24*, 339–346.

Mann, P. (2007), Global catalogue, classification and tectonic origins of restraining- and releasing bends on active and ancient strike-slip fault systems, in *Tectonics of Strike-Slip Restraining and Releasing Bends*, edited by W. D. Cunningham and P. Mann, *Geol. Soc. Spec. Publ.*, *290*, 13–142, doi:10.1144/SP290.2.

Mann, P., M. R. Hempton, D. C. Bradley, and K. Burke (1983), Development of pull-apart basins, *J. Geol.*, *91*, 529–554, doi:10.1086/628803.

Militzer, H., and F. Weber (1984), *Angewandte Geophysik, Bd. 1: Gravimetrie und Magnetik*, 353 pp., Springer, Berlin.

Peresson, H., and K. Decker (1997), Far-field effects of Late Miocene subduction in the Eastern Carpathians: E-W compression and inversion of structures in the Alpine-Carpathian-Pannonian region, *Tectonics*, *16*, 38–56, doi:10.1029/96TC02730.

Prohaska, W. (1983), Die geologischen und hydrogeologischen Verhältnisse am Westrand des südlichen Wiener Beckens, PhD Thesis, 161 pp., Univ. of Vienna, Vienna.

Rahe, B., D. Ferril, and A. Morris (1998), Physical analog modeling of pull-apart basin evolution, *Tectonophysics*, *285*, 21–40, doi:10.1016/S0040-1951(97)00193-5.

Rajchl, M., D. Uličný, R. Grygar, and K. Mach (2009), Evolution of basin architecture in an incipient continental rift: The Cenozoic Most Basin, Eger Graben (Central Europe), *Basin Res.*, *21*, 269–294, doi:10.1111/j.1365-2117.2008.00393.x.

Ratschbacher, L., O. Merle, P. Davy, and P. Cobbold (1991a), Lateral extrusion in the eastern Alps, part I: Boundary conditions and experiments scaled for gravity, *Tectonics*, *10*, 245–256, doi:10.1029/90TC02622.

Ratschbacher, L., W. Frisch, and H. G. Linzer (1991b), Lateral extrusion in the eastern Alps, part II: Structural analysis, *Tectonics*, *10*, 257–271, doi:10.1029/90TC02623.

Reinecker, J., and W. Lenhardt (1999), Present-day stress field and deformation in eastern Austria, *Int. J. Earth Sci.*, *88*, 532–550, doi:10.1007/s005310050283.

Reynisson, R. F., J. Ebbing, and J. R. Skilbrei (2007), Magnetic and gravity field in an integrated approach to the sub-basalt imaging problem, paper presented at EGM 2007 International Workshop, Eur. Assoc. of Geosci. and Eng., Capri, Italy, 15–18 Apr.

Roštínský, P., B. Roetzel, and R. Roetzel (2005), Exhumed Cenozoic landforms on the SE flank of the Bohemian Massive in the Czech Republic and Austria, *Z. Geomorphol.*, *49*, 23–45.

Rotstein, Y., J.-B. Edel, G. Gabriel, D. Boulanger, M. Schaming, and M. Munschy (2006), Insight into the structure of the Upper Rhine Graben and its basement from a new compilation of Bouguer Gravity, *Tectonophysics*, *425*, 55–70, doi:10.1016/j.tecto.2006.07.002.

Rousset, D., R. Bayer, D. Guillon, and J.-B. Edel (1993), Structure of the southern Rhine Graben from gravity and reflection seismic data, *Tectonophysics*, *221*, 135–153, doi:10.1016/0040-1951(93)90329-I.

Royden, L. H. (1985), The Vienna Basin: A thin-skinned pull-apart basin, in *Strike Slip Deformation, Basin Formation and Sedimentation*, edited by K. T. Biddle and N. Christie-Blick, *Spec. Publ. SEPM (Soc. Sediment. Geol.)*, *37*, 319–338.

Royden, L. H., F. Horváth, and B. C. Burchfiel (1982), Transform faulting, extension, and subduction in the Carpathian Pannonian region, *Geol. Soc. Am. Bull.*, *93*, 717–725, doi:10.1130/0016-7606(1982)93<717:TFEASI>2.0.CO;2.

Salcher, B. C. (2008) Sedimentology and modeling of the Mitterndorf Basin, PhD thesis, Univ. of Vienna, Vienna.

Salcher, B. C., and M. Wagreich (2010), Climate and tectonic controls on Pleistocene sequence development and river evolution in the Southern Vienna Basin (Austria), *Quat. Int.*, *222*, 154–167, doi:10.1016/j.quaint.2009.04.007.

Salcher, B. C., R. Faber, and M. Wagreich (2010), Climate as main factor controlling the sequence development of two Pleistocene alluvial fans in the Vienna Basin (eastern Austria)—A numerical modelling approach, *Geomorphology*, *115*, 215–227, doi:10.1016/j.geomorph.2009.06.030.

Sauer, R., P. Seifert, and G. Wessely (1992), Guidebook to excursion in the Vienna Basin and the adjacent Alpine-Carpathian thrustbelt in Austria, *Mitt. Oesterr. Geol. Ges.*, *85*, 1–264.

Schenková, Z., M. Kovac, D. Plasienka, and M. Sujan (1998), Seismogenic zones in Eastern Alpine-Western Carpathian-Pannonian junction area, *Geol. Carpathica*, *49*, 247–260.

Schlische, R. W., M. O. Withjack, and G. Eisenstadt (2002), An experimental study of the secondary deformation produced by oblique-slip normal faulting, *AAPG Bull.*, *86*, 885–906.

Sedlák, J., J. Blimka, H. Granser, V. Szalaiová, and B. Šály (2001), Gravity images of the Viennese Basin and surrounding petroliferous areas, *Proc. 8th Int. Meeting on Alpine Gravimetry, Leoben 2000*, *Osterr. Beitr. Meterol. Geophys.*, *26*, 137–144.

Shepard, D. (1968), A two-dimensional interpolation function for irregularly spaced data, in *Proceedings of the 1968 ACM National Conference*, pp. 517–524, Assoc. for Comp. Mach., New York.

Smit, J., J.-P. Brun, S. Cloetingh, and Z. Ben-Avraham (2008), Pull-apart basin formation and development in narrow transform zones with application to the Dead Sea Basin, *Tectonics*, *27*, TC6018, doi:10.1029/2007TC002119.

Smit, J., J.-P. Brun, S. Cloetingh, and Z. Ben-Avraham (2010), The rift-like structure and asymmetry of the Dead Sea Fault, *Earth Planet. Sci. Lett.*, *290*, 74–82, doi:10.1016/j.epsl.2009.11.060.

Szafián, P., and F. Horváth (2006), Crustal structure in the Carpatho-Pannonian region: Insights from three-dimensional gravity modeling and their geodynamic significance, *Int. J. Earth Sci.*, *95*, 50–67, doi:10.1007/s00531-005-0488-x.

Tari, G., F. Horváth, and J. Rumpler (1992), Styles of extension in the Pannonian Basin, *Tectonophysics*, *208*, 203–219, doi:10.1016/0040-1951(92)90345-7.

Ten Brink, U. S., Z. Ben-Avraham, R. E. Bell, M. Hassouneh, D. F. Coleman, G. Andreasen, G. Tibor, and B. Coakley (1993), Structure of the Dead Sea Pull-Apart Basin from gravity analyses, *J. Geophys. Res.*, *98*, 21,877–21,894, doi:10.1029/93JB02025.

Unterwelz, H. (1993), Structural map of the Top Sarmatian Horizon in the Vienna Basin, in *Erdöl und Erdgas in Österreich*, edited by F. Brix and O. Schultz, Suppl. map 2, Mus. of Nat. Hist., Vienna.

Wakabayashi, J. (2007), Stepovers that migrate with respect to affected deposits: Field characteristics and speculation on some details of their evolution, in *Tectonics of Strike-Slip Restraining and Releasing Bends*, edited by W. D. Cunningham and P. Mann, *Geol. Soc. Lond. Spec. Publ.*, *290*, 169–188, doi:10.1144/SP290.4.

Wakabayashi, J., J. V. Hengesh, and T. L. Sawyer (2004), Four-dimensional transform fault processes: Progressive evolution of step-overs and bends, *Tectonophysics*, *392*, 279–301, doi:10.1016/j.tecto.2004.04.013.

Wessely, G. (1961), Geologie der Hainburger Berge, *Jahrb. Geol. Bundesanst.*, *104*, 273–349.

Wessely, G. (1979), The structural map of the Leopoldsdorf fault, map, scale 1:50:000, OMV, Vienna.

Wessely, G. (1988), Structure and development of the Vienna Basin in Austria, in *The Pannonian Basin: A Study in Basin Evolution*, edited by L. H. Royden and F. Horváth, *AAPG Mem.*, *45*, 333–346.

Wessely, G. (2006), *Geologie der österreichischen Bundesländer, Niederösterreich*, Geol. Surv. of Austria, Vienna.

Wu, J. E., K. McClay, P. Whitehouse, and T. Dooley (2009), 4D analogue modeling of transtensional pull-apart basins, *Mar. Pet. Geol.*, *26*, 1608–1623, doi:10.1016/j.marpetgeo.2008.06.007.

Zámolyi, A., B. Székely, E. Draganits, and G. Timár (2010), Neotectonic control on river sinuosity at the western margin of the Little Hungarian Plain, *Geomorphology*, *122*, 231–243, doi:10.1016/j.geomorph.2009.06.028.

Zeng, H. (1989), Estimation of the degree of polynomial fitted to gravity anomalies and its application, *Geophys. Prospect.*, *37*, 959–973, doi:10.1111/j.1365-2478.1989.tb02242.x.

Zych, D., B. Meurers, and P. Steinhauser (1993), Gravity map of the Vienna Basin and adjacent areas, Austrian Geol. Surv., Vienna.